

SolarNet: A hybrid reliable model based on convolutional neural network and variational mode decomposition for hourly photovoltaic power forecasting

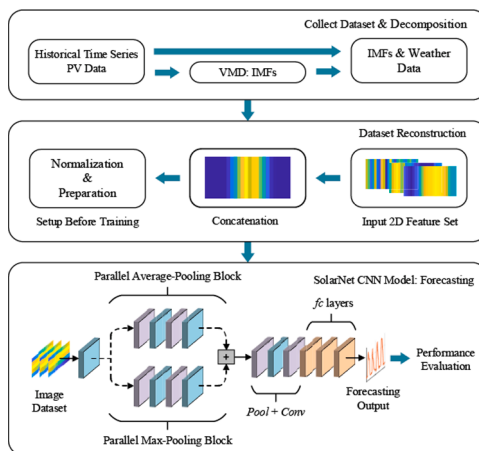
Deniz Korkmaz

Malatya Turgut Ozal University, Faculty of Engineering and Natural Sciences, Department of Electrical and Electronics Engineering, Malatya 44210, Turkey

HIGHLIGHTS

- Parallel pooling structure-based network exhibits superior forecasting performance.
- A new data reconstruction method extracts more distinguishing input features.
- Designed deep forecasting network has a low computational cost and complexity.
- Forecasting experiments are verified in different weather conditions and all seasons.
- Proposed method outperforms various other state-of-the-art deep learning models.

GRAPHICAL ABSTRACT



ARTICLE INFO

Keywords:

Photovoltaic power forecasting
Convolutional neural network
Parallel pooling
Variational mode decomposition
Deep learning

ABSTRACT

Photovoltaic (PV) power generation has high uncertainties due to the randomness and imbalance nature of solar energy and meteorological parameters. Hence, accurate PV power forecasts are essential in the operation of PV power plants (PVPP) for short-term dispatches and power generation schedules. In this study, a novel convolutional neural network (CNN) model, namely SolarNet, is proposed for short-term PV output power forecasting under different weather conditions and seasons. The proposed CNN model is designed as a parallel pooling structure to increase the forecasting performance. This structure consists of max-pooling and average-pooling blocks. The input parameters are the measured historical solar radiation, temperature, humidity, and active power data. The power data is decomposed into sub-components with the variational mode decomposition method and a data preprocessing and reconstruction process is utilized to obtain deep input feature maps. After input parameters are converted to hue-saturation-value (HSV) color space, the subsets feed to the input of the network. The experimental studies are performed with a case study using a 23.40 kW PVPP dataset from the Desert Knowledge Australia Solar Centre. The design CNN model is also compared with benchmark deep learning methods. In the experiments, the average correlation coefficient (R), root mean square error (RMSE), and mean

E-mail address: deniz.korkmaz@ozal.edu.tr.

<https://doi.org/10.1016/j.apenergy.2021.117410>

Received 15 February 2021; Received in revised form 9 June 2021; Accepted 7 July 2021

Available online 15 July 2021

0306-2619/© 2021 Elsevier Ltd. All rights reserved.

absolute error (MAE) of the proposed method for 1-h different weather conditions are achieved as 0.9871, 0.3090, and 0.1750, respectively. The experimental results show that the proposed deep forecasting method has higher accuracy and stability in short-term PV power forecasting and outperforms the other deep learning methods.

Nomenclature	
<i>Abbreviation</i>	
ADMM	Alternate Direction Method of Multipliers
ANN	Artificial Neural Network
ARIMA	Autoregressive Integrated Moving Average
ARMA	Autoregressive and Moving Average
BN	Batch Normalization
CNN	Convolutional Neural Network
DKASC	Desert Knowledge Australia Solar Center
DT	Decision Tree
EEMD	Ensemble Empirical Mode Decomposition
ELM	Extreme Learning Machine
EMD	Empirical Mode Decomposition
fc	Fully Connected
GA	Genetic Algorithm
GPR	Gaussian Process Regression
HIMVO	Hybrid Improved Multi-verse Optimizer
HSV	Hue-Saturation-Value
IMF	Intrinsic Mode Function
L-ReLU	Leaky Rectified Linear Unit
LSTM	Long Short Term Memory
MAE	Mean Absolute Error
Max	Maximum
Med	Median
Min	Minimum
NWP	Numerical Weather Prediction
Pctl	Percentiles
ps	Pixel Size
PV	Photovoltaic
PVPP	Photovoltaic Power Plant
R	Correlation Coefficient
RCC	Radiation Classification Coordinate
ReLU	Rectified Linear Unit
RES	Renewable Energy Source
RF	Random Forest
RGB	Red-Green-Blue
RMSE	Root Mean Square Error
RNN	Recurrent Neural Network
SDA	Similar Day Analysis
SGD	Stochastic Gradient Descent
Std	Standard Deviation
SVM	Support Vector Machine
SVR	Support Vector Regression
VMD	Variational Mode Decomposition
WT	Wavelet Transform
2D	Two-Dimensional

1. Introduction

With the global warming and depletion of fossil fuels in recent years, renewable energy sources (RESSs) such as solar, wind, hydroelectric, and geothermal energy have started to reflect the future of energy conversions. Besides the environmental benefits, the enormous increase in load demand has also increased the interest of RESSs [1–3]. The European Union aims to generate 30% and 100% of its total energy from RESSs by 2030 and 2050 [4]. Renewable energy can be integrated into various units from large-scale stations integrated into transmission power systems to units integrated into low-voltage distribution systems. One of the remarkable RES types is solar energy systems. Solar energy has become a more admissible and promising energy source due to its enormous potential power and easy availability [5,6]. Compared with conventional energy sources, solar energy has many advantages such as abundant resources, wide distribution, no pollution, free use, and ease of transportation. One of the significant features is also that the world energy consumption need for a day is less than the amount of energy taken from the sun. Therefore, investors, governments, and international organizations have increasingly interested in solar energy systems [7,8].

Generally, solar power generation can be provided with thermal and photovoltaic (PV) systems. Among them, PV is considered one of the most promising power generation techniques that give clean and sustainable energy. With the continuous development of PV power generation, PV electricity networks have increased day by day [3,9]. According to the Renewables Global Status Report 2019 [10], more than 181 GW of new renewable energy systems have been constructed around the world and nearly 55% of them are PV power plants (PVPPs). However, PVPPs are typical fluctuating sources and have strong uncertainties

and variabilities due to the chaotic and unsteady nature of the weather conditions. The variability of PV power generation may cause volatility and randomness that affects integrated power grids. These natural characteristics of the PV systems lead to new challenges to the management and operation of PVPPs and decrease the real-time control performance. The accurate forecasting of PV power generation is one of the key solutions to determine the proper operational schedule and short-term dispatch planning. Besides, an effective forecasting process can ensure reliability, reduction of potential operation costs, and increased penetration levels [10,11].

According to the time scale of forecasts, forecasting of PV power generation can be categorized into very-short-term, short-term, medium-term, and long-term forecasts. The prediction interval can be determined from a minute to over a year. For a medium or long-term forecast, high errors can be encountered due to the randomness and uncertainties in the long time intervals, and these forecast horizons are mainly used for the long-term planning of power grids. In order to determine real-time dispatches, maintenance planning, and operations of the power grid markets, high forecasting accuracy and minimum error are needed. Among these horizons, short-term forecasting is a significant way and it can provide effective results to obtain better planning to market players. Therefore, interest in very-short and short-term PV power forecasting has rapidly been increased and become a popular topic in this area [7,10,12].

1.1. Related works

Generally, PV power forecasting methods are divided into three main categories as physical, statistical, and soft computing methods [3,8]. The physical method depends on a mathematical model that includes the geographical states of PV plant, principles of PV power generation, and

weather conditions as solar radiation, humidity, temperature, cloud volume, rainfall, and wind speed. Weather conditions of the system are obtained from the numerical weather prediction (NWP) process. For this method, historical time-series data are not required but detailed geological state of the plant, accurate meteorological weather data, and PV battery specifications are used. Although the forecasting accuracy highly depends on the NWP results, NWP performance may be reduced in some cases. In addition, the correlation between the model and PV panel is obtained with errors, the whole model is complex, and the computational cost is high [1,7]. Statistical methods commonly include regression analysis [13], auto-regressive moving average (ARMA) [14], and autoregressive integrated moving average (ARIMA) [15]. Statistical methods are simpler than physical methods and can achieve more accurate forecasting results because historical PV data are used and model parameters are optimized. However, statistical forecasting methods still have some obvious shortcomings. They require a steady correlational mapping between inputs and outputs, and forecasting accuracy can be lower on rainy and cloudy days [3]. There is a precondition that needs to handle a large number of historical data. This process can be a challenge during the data acquisition and training process [7]. The high performance of the statistical methods depends on the quality and detailed PV data [10]. In addition, they cannot extract deep features belong to the inputs and PV power. The most remarkable of the above methods is soft computing-based forecasting methods. Soft computing methods can overcome some problems that conventional approaches are not able to solve. The ability to exhibit a relationship between inputs and outputs makes these methods a highly effective tool for data mining and forecasting problems. Soft computing methods are commonly employed to extract the nonlinear and high-dimensional features belong to the PV systems and have the ability to map them to the outputs. These features can further improve forecasting accuracy. With their effective properties of the soft computing methods, they have become the most popular approaches to predict time-series data. As a result, soft computing-based forecasting methods always provide a more competitive performance than physical and statistical methods [7,8,16].

Various soft computing methods have been examined in PV power forecasts, which have different characteristics. Support vector regression (SVR) is a popular method in this field. Eseye et al. [17] developed a decomposition and optimization-based SVR model to forecast short-term PV power generation. Li et al. [18] proposed a hybrid improved multi-verse optimizer algorithm to obtain the best SVR parameters for PV forecast systems. Das et al. [19] used a SVR model to forecast PV power under different weather conditions. However, the SVR method requires an optimization algorithm and cross-validation to determine the hyper-parameters and to improve the forecasting accuracy. Gaussian process regression (GPR) is another method in grid-connected PV systems and utilizes Bayesian optimization to adjust adaptive hyper-parameters [20]. The main disadvantage of this method is the difficulty of calculating high-dimensional data. Random forest (RF) and decision tree (DT) ensemble algorithms are also a kind of forecasting method [21,22]. Nevertheless, proper data is needed and big data forecasting performances are weak in harsh weather conditions. Another frequently used method is artificial neural networks (ANNs). Mellit et al. [23] proposed an ANN model by using historical meteorological data and they obtained better performance than typical physical and statistical methods. Zhou et al. [24] employed an extreme learning machine (ELM), which is a feedforward neural network, to predict hourly PV power output. However, these neural network models are shallow techniques in this area due to their leaky prediction ability in harsh weather conditions. Furthermore, traditional networks may cause overfitting and gradient disappearance.

On the contrary above methods, deep learning models have higher feature extraction capabilities than traditional neural networks and regression methods to achieve more accurate forecasting results. Abdel-Nasser and Mahmoud [2] developed the window technique-based long-short term memory (LSTM)-recurrent neural network (RNN) model and

modeled the temporal changes. In [7,9], day-ahead PV power forecasting was evaluated with convolutional neural network (CNN), RNN, LSTM, and hybrid models. In the experiments, hybrid structures outperformed the other models. In another study, the day-ahead PV power forecasting approach was given using pre-trained CNN models [3]. Although the obtained results are better, the used networks have large learnable parameters and extreme training times. Zang et al. [25] proposed a hybrid CNN model and different frequency components were decomposed from historical data with empirical mode decomposition (EMD). The designed model outperformed various traditional regression methods with diverse capacities in various hourly timescales. Lee et al. [26] used a CNN-LSTM model to forecast from 1-h to 6-h horizons in 14 sites in South Korea and obtained an average root mean square error (RMSE) of 0.1542. Wang et al. [27] presented a wavelet decomposition-based CNN-LSTM model for day-ahead solar irradiance forecasting. The CNN model was used to extract deep features and the results also compared with ANN and traditional CNNs. Sun et al. [28] designed a sky images-based CNN model to forecast PV power and achieved a relative-RMSE of 26% to 30.2% for two solar PV systems. However, collect of the required data is challenging due to the structure of the constructed system. Aprillia et al. [29] proposed a short-term PV power forecasting approach with a salp swarm algorithm-based CNN model. Various forecasting models of CNN regression were established to accommodate the prediction for different weather types. In a different study, mid-to-long-term wind and PV power generations were predicted with a copula function-based LSTM model [30]. Copula function was used to find the correlation between meteorological factors and power generation and extracted the significant meteorological factors affecting the power generation.

1.2. Research gaps and scientific contributions

For the above existing studies, there are still some issues and need to further researches. Previous conventional studies have mainly focused on structural improvements. In these models, accurate and robust forecasting results cannot be obtained when the time-series data is directly applied to the model, especially on cloudy and rainy days. Due to the nature of the weather data, the original PV output power is highly nonlinear and nonstationary, and the conventional models may cause over-fitting and local minimization problems [31].

Recent studies have emphasized the CNN-based methods to improve the forecasting performance of RESs. CNNs are a type of deep neural network with convolutional layers and have state-of-the-art performance in many high-level problems related to nonlinear data. There are three main advantages: (I) They exhibit robust nonlinear generalization and representation capabilities in big data. (II) They can obtain higher learning abilities with extracted deep features in inputs. (III) They can also utilize inputs in various ways by transforming the input data into images [1,32]. These significant advantages show that CNNs can provide to learn more distinguishing and effective features in PV forecasting problems compared to shallow learning architectures. Therefore, CNN architectures can significantly overcome the forecasting problems and exhibit promising results [26,33]. However, there are some gaps in the literature. Firstly, the accuracies of conventional CNN and LSTM models can be improved with the rapid development of deep learning architectures to provide the reliability and robustness for proper operational schedules. Secondly, LSTM models may not be a proper solution when considering the complexity of the model and accuracy [34]. Thirdly, complex CNN models have enormous learnable parameters and the implementation is difficult in embedded-system applications. Finally, forecasting models should exhibit generalization capabilities by giving the high performance on cloudy and rainy days as in seasonal and periodic forecasts.

In addition, there are limited studies focusing on the usage of decomposition methods in PV power forecasting problems to obtain more comprehensive sub-power components. An effective time-series

decomposition method for the PV power derives the sub-components and can improve the performance of the forecasting model [25]. The decomposition can also reduce the effect of nonstationary factors on forecasting results with some approaches such as EMD [35], ensemble EMD (EEMD), variational mode decomposition (VMD) [36], and wavelet transform (WT) [31]. While the EMD and VMD methods have robust self-adaptability, WT decomposition can exhibit weak self-adaptability. VMD also handles good robustness and avoids typical mode aliasing problems of EMD and EEMD. Since the VMD method has been used in various forecasts of renewable energy systems [36,37], the PV power is decomposed with the VMD method in the present paper.

To bridge the aforementioned gaps, a novel and effective CNN architecture-based PV power forecasting method (SolarNet) is proposed in this paper. In order to improve the short-term forecasting performance and simplify the deep learning model, a parallel pooling structure is designed with few self-parameters and strong generalization ability. This structure utilizes two parallel blocks as max-pooling and average-pooling. The proposed framework includes four main stages as decomposition with the VMD, reconstruction of the historical time-series inputs into the hue-saturation-value (HSV) color space and concatenation into a single red-greenblue (RGB) image, training of the designed CNN model, and testing phase of the trained network. The VMD method decomposes the historical power data into sub-components. Afterward, all of the input data are converted to two-dimensional (2D) input images to extract more comprehensive nonlinear features by the convolutions. The input parameters of the network are the measured historical global horizontal radiation, diffuse horizontal radiation, temperature, humidity, and active power of the technology demonstration facility in Australia. The SolarNet structure is intended to improve the forecasting performance by incorporating seasonal and periodic patterns, and also diverse weather conditions into the testing phase for PV power at any candidate site. Contrary to those existing methods, it is also aimed to train the deep neural network and utilize the extracted convolutional features, rather than directly forecast PV power. Therefore, this paper contributes to the existing literature in solar power generation by analyzing the effectiveness of the hybrid architecture with the VMD method and image construction process. The proposed network is evaluated with the single pooling structures and various deep learning models. The obtained results are also compared with the existing state-of-the-art studies to evaluate the effectiveness of the designed CNN model. **The novelty and main contributions of this paper can be summarized as follows:**

- **A novel parallel pooling structure-based CNN model is proposed to achieve robust, generalized, and high forecasting performance in PV power generation.** The proposed SolarNet is a combination of the pooling layers that represent the multiscale deep features with different levels of visual perception.
- **The decomposition and reconstruction processes are applied.** The VMD algorithm reduces the instability and non-linearity of the raw power data and derives the intrinsic modes to improve the forecasting accuracy. The data reconstruction process of multi-channels is utilized with correlations in both daily and hourly timescales to achieve sufficient performance. This process constructs input features and extracts the advanced features by reducing the information vanishing problem.
- **A simple, rapid, and efficient CNN architecture is designed for solar energy systems.** The designed CNN model has less learnable parameters and high forecasting performance. Therefore, it can be applicable in grid-connected systems to determine the proper operational schedule and short-term dispatch planning.
- **The experimental results are evaluated with state-of-the-art deep learning models on seasonal and diverse weather conditions.** It is confirmed that the proposed method outperformed the most-known deep learning models and related existing studies.

The other sections of this paper are presented as follows: [Section 2](#) describes background theories. [Section 3](#) expresses the framework of the proposed forecasting method. The experiments and findings of the study are given in [Section 4](#). Finally, the conclusion of the study is briefed in [Section 5](#).

2. Background theories

CNN architectures are extremely effective methods in image-related problems due to their strong feature extraction capabilities. CNNs consist of a series of convolutional, pooling, and nonlinear operations, and these structures have the following characteristics: (I) A convolutional layer utilizes spatially local connectivity patterns between the neighboring layers. (II) Each filter is repeated across the whole visual field to reduce the number of network parameters. (III) The multilayer structure provides multi-level features. (IV) The feature extraction process is adapted into one framework to provide more suitable learned features for any specific task [32,38]. Therefore, those characteristics can achieve promising results than data-driven learned features with traditional regression methods. In this paper, a novel and effective CNN architecture for the PV power forecasting method is proposed. The designed procedure depends on the above-mentioned characteristics and three main preliminaries are determined as robustness, high accuracy, and computational efficiency. For the renewable energy power forecasting problems, the robustness ensures a more competitive performance avoiding seasonal effects due to changing meteorological factors. High forecasting accuracy can help to provide reliability and reduction of potential operation costs. In addition, low computational complexity is required to easily handle large-scale PV datasets.

The following subsections describe the VMD method, data pre-processing and reconstruction process, and parallel pooling structure-based SolarNet architecture in detail.

2.1. Variational mode decomposition

The output of the PV systems fluctuates with uncertain frequencies. In order to avoid the overfitting of the training process and improve the forecasting accuracy, the time-series PV power data is decomposed through the VMD method. This algorithm is a non-recursive signal processing method that can decompose time-series data into a series of intrinsic mode functions (IMFs) with specific bandwidth. Each IMF can be formed around a determined center frequency and bandwidth, and the sum value of the bandwidth is minimized [39,40]. Contrary to EMD and EEMD, the VMD method can prevent iterative computation by generating a cycling scanning process at different frequencies. Therefore, VMD is a more robust decomposition method against noise [25]. In this method, the bandwidth of each mode u_k is derived with the following process:

Hilbert transform is applied to decompose the PV power time-series data $P(t)$ for each mode u_k as below:

$$\left(\delta(t) + \frac{j}{\pi t} \right)^* u_k(t) \quad (1)$$

For each mode, an exponential tuning operator $e^{-jw_k t}$ is used to modulate the frequency spectrum of mode to the baseband by the following equation:

$$\left[\left(\delta(t) + \frac{j}{\pi t} \right)^* u_k(t) \right] e^{-jw_k t}. \quad (2)$$

Estimation of the bandwidth of each mode is obtained with H^1 Gaussian smoothness of the demodulated signal.

After the bandwidth estimation, the constrained variational problem is given as (3):

$$\min_{(u_k, w_k)} \left\{ \sum_{k=1}^N \left\| \partial_t \left[\left(\delta(t) + \frac{j}{\pi t} \right)^* u_k(t) \right] e^{-jw_k t} \right\|_2^2 \right\} \quad (3)$$

s.t. $P(t) = \sum_{k=1}^N u_k$

Here, u_k is the k th mode and represents the set of modes as $\{u_k\} = \{u_1, u_2, \dots, u_N\}$. w_k is the k th center frequency of u_k i.e. $\{w_1, w_2, \dots, w_N\}$. $(\cdot)^*$ is the convolution operation and $\delta(t)$ defines the Dirac distribution. With a quadratic balancing parameter α and Lagrangian multipliers λ , the constrained variational problem can be given as an unconstrained variational problem, as shown in (4):

$$L(u_k, w_k, \lambda) = \alpha \sum_{k=1}^K \left\| \partial_t \left[\left(\delta(t) + \frac{j}{\pi t} \right)^* u_k(t) \right] e^{-jw_k t} \right\|_2^2 + \|P(t) - \sum_{k=1}^K u_k(t)\|_2^2 + \left\langle \lambda(t), P(t) - \sum_{k=1}^K u_k(t) \right\rangle. \quad (4)$$

Therefore, the above-mentioned problem is solved using the alternate direction method of multipliers (ADMM) and (u_k, w_k) is updated in two directions. Consequently, the solutions are expressed as (5) and (6) for all $w \geq 0$:

$$\hat{u}_k^{n+1} = \frac{\hat{P}(w) - \sum_{i \neq k} \hat{u}_i(w) + \frac{\hat{\lambda}(w)}{2}}{1 + 2\alpha(w - w_k)^2}. \quad (5)$$

$$w_k^{n+1} = \frac{\int_0^\infty w \left| \widehat{y}_k^{n+1}(w) \right|^2 dw}{\int_0^\infty \left| \widehat{y}_k^{n+1}(w) \right|^2 dw}, \quad (6)$$

where n is the iteration number and (\cdot) represents the Fourier transform. As a result, $\hat{P}(w)$, $\hat{u}_i(w)$, $\hat{\lambda}(w)$, and \hat{u}_k^{n+1} are the Fourier transforms of $P(t)$, $u_i(t)$, $\lambda(t)$, and $u_k^{n+1}(t)$, respectively. Here, the iteration is completed when the convergence criterion (ϵ) is achieved with:

$$\sum_{k=1}^K \left\| \hat{u}_k^{n+1} - \hat{u}_k^n \right\|_2^2 / \left\| \hat{u}_k^n \right\|_2^2 < \epsilon \quad (7)$$

According to the above descriptions, the obtained PV power modes and residual reduce the instability and non-linearity of the original data as shown in Fig. 1. The norm of the difference between the original and the decomposed functions gives the decomposition performance and it is calculated as $0.011e-14$. The IMF and residual components include the daily and hourly correlations of all years.

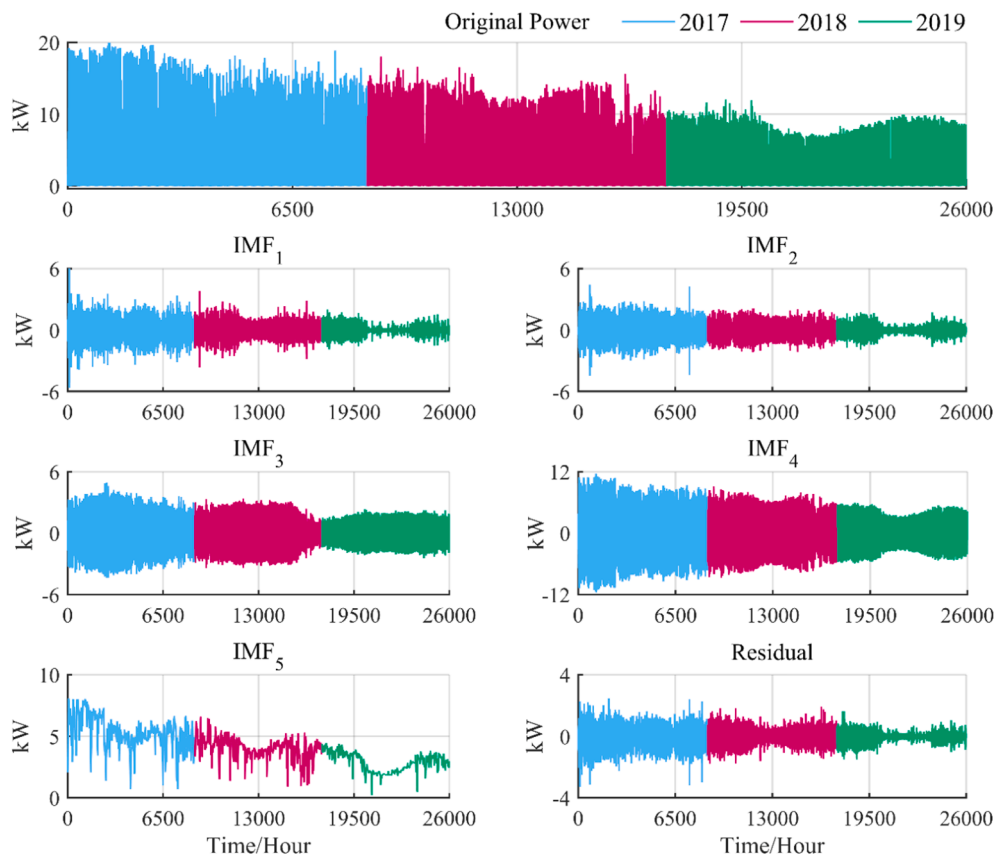


Fig. 1. Obtained sub-power components from the VMD method.

2.2. Data preprocessing and reconstruction process

The data preprocessing and reconstruction process is a quite significant factor that converts historical data into 2D input images. This process allows the designed SolarNet structure to be easily used rather than recurrent neural networks and one-dimensional CNN models. As visual patterns are constructed, the inherent spatial invariance of the network provides better learning with optimal inputs. In this process, historical data is defined as the input while PV output power is defined as the output. The preprocessing and reconstruction consists of four sub-process as normalization, transformation to 2D HSV color space, concatenation of the inputs, and construction of the sub-set data for CNN inputs.

In order to build input images, each time-series input $x_{i,k}(t)$ is converted into HSV color space and represented as an RGB image with 5×24 resolution and 8-bit depth in a 3-channel matrix. Hence, the input feature maps can be defined as $F_{i,k}$. Here, i and k represent the number of inputs with $i = 1, 2, \dots, N$ and the sample of each element with $k = 1, 2, \dots, M$, respectively. N and M are the number of total inputs and samples, respectively. Once the input feature maps are obtained, they are concatenated with the associated samples. As each sample shows the change in data, the concatenation aims at building a unique image. Let $F_{i,k}$ has $r_1 \times r_2$ pixel size and I_k is the concatenated image. The building of new images is performed by concatenating the r_2 pixels of the inputs and the new pixel size (ps) is given as below [41,42]:

$$ps(I_k) = F_{i,k}(r_1) \times \sum_{i=1}^N F_{i,k}(r_2) \quad (8)$$

Finally, input images of the network are obtained as a single RGB image and give the new input set. An example of the whole process is shown in Fig. 2. The inputs are selected as 1×24 resolution (one-day data) to give more detail on the changes of power and weather conditions on a day. The new input set is also resized to 150×72 dimensions with RGB channels to increase the learning of convolutions. The changes of the pixel points are quite stable and each image ensures comprehensive daily and hourly correlations. After the reconstruction process, all images are randomly divided into training and validation subset data.

Furthermore, the PV output power data is rescaled to achieve better training performance. Let $P = \{p_1, p_2, \dots, p_M\}$ is the considered time-series output data with M component. Therefore, each sample of P is normalized with center 0 and standard deviation 1 as follows;

$$\tilde{P} = \frac{(P - \eta)}{\sigma} \quad (9)$$

where η and σ are the mean and standard deviation of P , respectively. Finally, the scaled data is represented with $\tilde{P} = \{\tilde{p}_1, \tilde{p}_2, \dots, \tilde{p}_M\}$ and the subset of the output can be prepared.

2.3. Parallel pooling structure-based CNN architecture

In the proposed deep PV forecasting method, a simple and effective CNN model is constructed with a parallel pooling structure [43] that fully utilizes image recognition and extracts high-level features from multiple convolutional layers. The specifications of the parallel structure ensure the multiscale deep features with different levels of visual

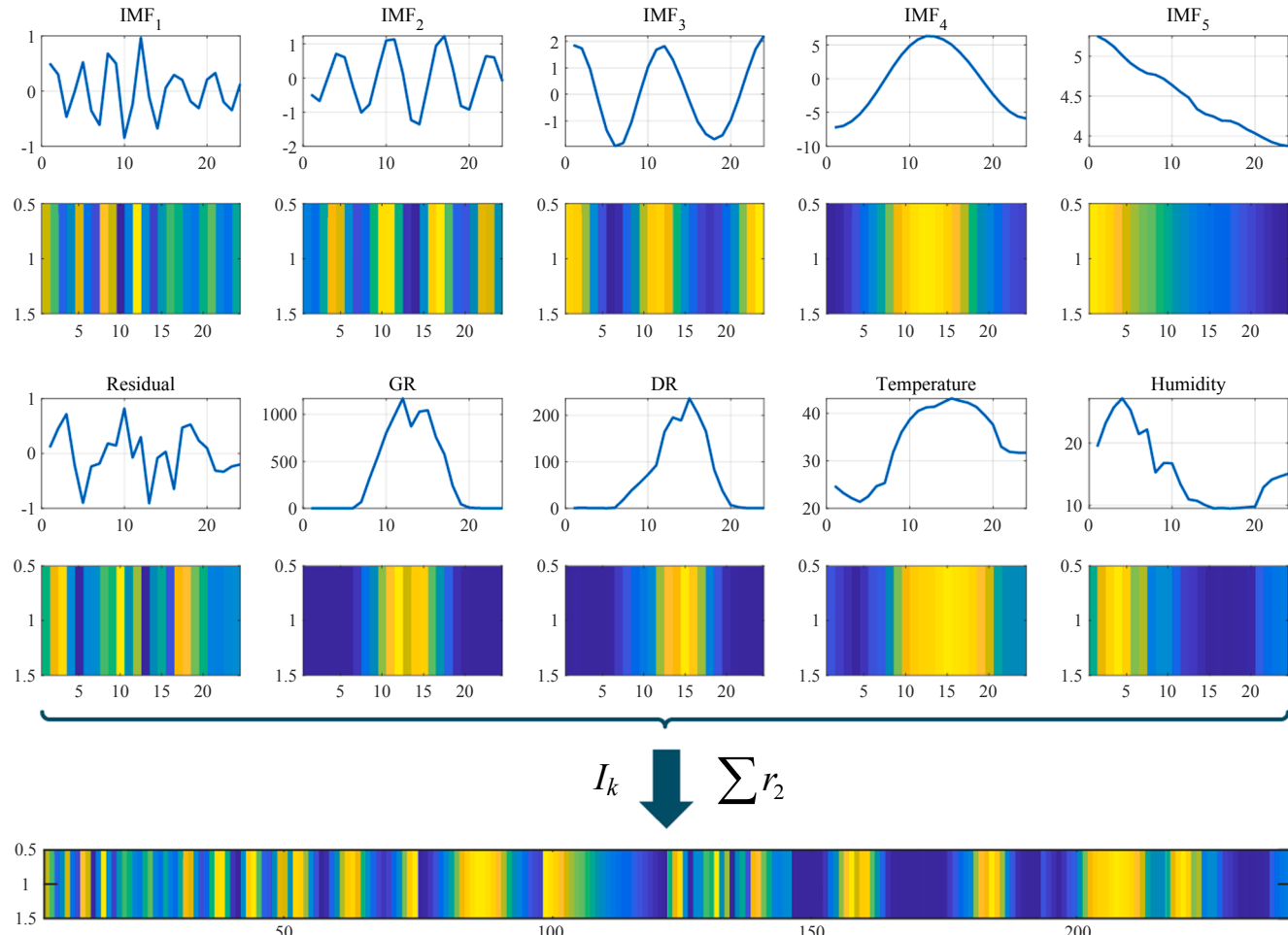


Fig. 2. HSV color space representation and reconstruction process of the input image for 1×24 resolution.

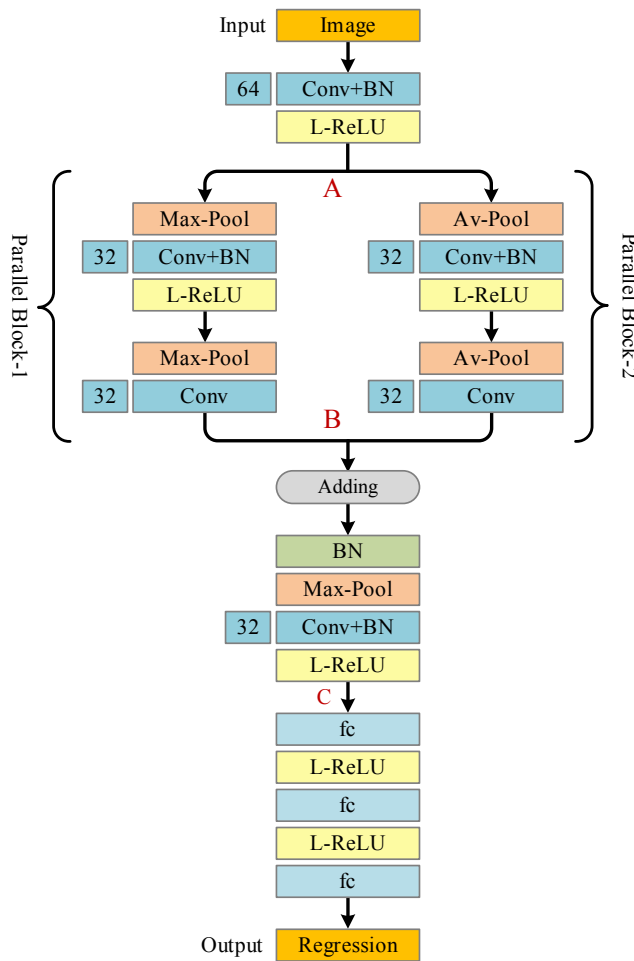


Fig. 3. Details on the designed CNN architecture based on the parallel pooling structure.

perception. As the parallel pooling retains features of the map required for forecasting through translational and rotational invariants, the CNN structure can be easily trained, and improved accuracy obtained. The designed network consists of fifteen layers with six convolution layers, three max-pooling, two average-pooling, three fully connected layers, and one regression layer. The detailed architecture of the network is presented in Fig. 3.

In the network, $\text{Conv}(k, s, D)$, $\text{Max-Pool}(k, s)$, $\text{Av-Pool}(k, s)$, $L\text{-ReLU}(\alpha)$, BN , and $fc(l)$ represent the convolutional, max-pooling, average-pooling, leaky rectified linear unit, batch normalization, and fully connected layers, respectively. It is noted that k is the kernel size, s is the stride, D is the output depth, α is the constant multiplier, and l gives the features. $L\text{-ReLU}$ is used to overcome the exploding and vanishing problems during gradient descent. The small-sized filters are selected and enable high-level feature maps to compute the output of the neurons. Firstly, a convolutional layer is utilized to extract low-level features from the images (from input to point A). The connections is given as: $\text{Input}(60 \times 40 \times 3) - \text{Conv}(5, 1, 64) - BN - L\text{-ReLU}(0.01)$. Then, low-level features are fed into two parallel blocks (from point A to point B). The parallel block structure provides more effective results by using two different pooling layers in situations where preserving localization is worse and it is given as: $\{\text{Max-Pool}(2, 2) - \text{Conv}(3, 1, 32) - BN - L\text{-ReLU}(0.01) - \text{Max-Pool}(2, 2) - \text{Conv}(3, 1, 32)\} // \{\text{Av-Pool}(2, 2) - \text{Conv}(3, 1, 32) - BN - L\text{-ReLU}(0.01) - \text{Av-Pool}(2, 2) - \text{Conv}(3, 1, 32)\}$ i.e. (Parallel Block-1 // Parallel Block-2). During back-propagation, pooling layers reduce the dimension of the outputs from the rectified unit with a statistic of nearby outputs. Max-Pool and Av-Pool find the maximum and average values for

each patch, respectively. Max-Pool operates the maximum operator with $\max(f_R)$, while Av-Pool operates the $\sum(f_R)/|f_R|$. Here, R is the pooling region. For the parallel structure, assume $\bar{I}_n \in \mathbb{R}^{B,D,r_1,r_2}$ is an input of a feature map with the number of batches B , output depth, and pixel size, and also parallel blocks operate with $\text{MaxConv}()$ and $\text{AvConv}()$ at stride s and padding p . To summarize, the output of the parallel pooling structure can be represented with the following equation:

$$\bar{y}(\bullet) = (\text{MaxConv}_n^{D,B}(\bar{I}_n) \oplus \text{AvConv}_n^{D,B}(\bar{I}_n)). \quad (10)$$

After this process, the sum of the trained feature maps $\sum \bar{y}(o)$ is fed into max-pooling with a convolution to extract deep features (from point B to point C). The detail is as follows: $BN - \text{Max-Pool}(2, 2) - \text{Conv}(3, 1, 32) - BN - L\text{-ReLU}(0.01)$. As a first element, the BN layer is used to reduce the noise level during training. Therefore, the learnable parameters can maintain the larger gradient state and increase the convergence speed.

According to the above expressions, the $\text{Conv}()$ layers compute the output of the neurons with filters to generate the feature maps. The convolution operation can be expressed by (11);

$$y_{n,j} = f_L \left(\sum_{n=1}^{k-1} \bar{I}_n * K_{n,j} + a_j \right). \quad (11)$$

where $f_L()$ is the $L\text{-ReLU}$ activation function and a_j is the adding bias vector of the j th neuron. The $L\text{-ReLU}$ function improves both learning speed and regression performance in the network with a more balancing form and it is given by:

$$f_L(t) = \begin{cases} 0.01t, & t < 0 \\ t, & t \geq 0 \end{cases}. \quad (12)$$

This function also applies the down-sampling operation to reduce the computational cost by decreasing the matrix size. Finally, the feature fusion process is completed and fed into the fully connected layers for

Table 1
Detailed layer configuration of the designed CNN architecture.

Layer	Type	#5 x 5	#3 x 3	#2 x 2	Stride	Output
Input	Image Input	–	–	–	–	$150 \times 72 \times 3$
Input Conv-1	Conv + BN + L-ReLU	64	–	–	1	$150 \times 72 \times 64$
Parallel Block-1	Max-Pooling	–	–	64	2	$75 \times 36 \times 64$
	Conv + BN + L-ReLU	–	32	–	1	$75 \times 36 \times 32$
	Max-Pooling	–	–	32	2	$38 \times 18 \times 32$
	Conv	–	32	–	1	$38 \times 18 \times 32$
Parallel Block-2	Average-Pooling	–	–	64	2	$75 \times 36 \times 64$
	Conv + BN + L-ReLU	–	32	–	1	$75 \times 36 \times 32$
	Average-Pooling	–	–	32	2	$38 \times 18 \times 32$
	Conv	–	32	–	1	$38 \times 18 \times 32$
Pool	BN + Max-Pooling	–	–	32	2	$19 \times 9 \times 32$
Serial Conv-6	Conv + BN + L-ReLU	–	32	–	1	$19 \times 9 \times 32$
fc-1	Fully Connected + L-ReLU	–	–	–	–	$1 \times 1 \times 100$
fc-2	Fully Connected + L-ReLU	–	–	–	–	$1 \times 1 \times 10$
fc-3	Fully Connected Regression Output	–	–	–	–	$1 \times 1 \times 1$

the PV power forecasting with distinctive features (from point C to regression output). Here, the obtained matrices are flattened and transferred to the following fully connected layers with L -ReLU functions. The final process is given as: $fc(100) - L$ -ReLU(0.01) - $fc(10)$ - L -ReLU(0.01) - $fc(1)$ - Regression(1, n).

As given in Eq. (11), fully connected layer multiples the input y_j by a weight matrix $w_{(n,j)}$, and the output is added to a bias vector:

$$fc(y_{n,j}) = a_j + \sum_{n=1}^{k-1} w_{n,j} \times y_j. \quad (13)$$

In the network output, a regression layer is used and the obtained high-level deep features are employed to forecast PV output power at time-series form. Table 1 summarizes the detailed layer configuration of the CNN architecture. It can be also noticed that an easy to implement CNN model is designed for embedded system applications to achieve

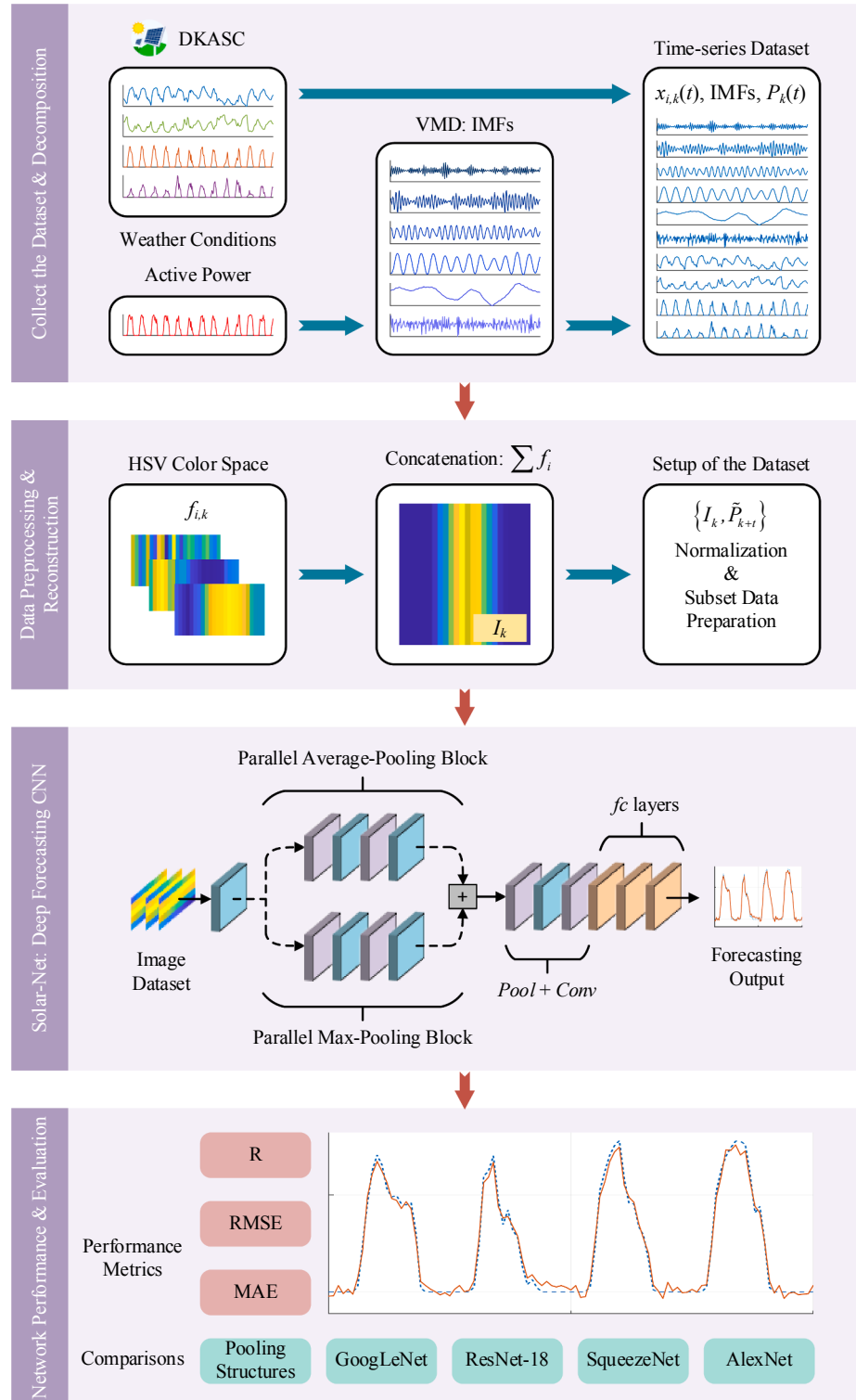


Fig. 4. Overall architecture of the parallel pooling structure-based deep PV power forecasting method.

high accuracy, fast forecasting speed, and good adaptability.

3. Framework of the proposed deep forecasting method

In the proposed forecasting method, an advanced and novel parallel pooling structure-based CNN model is designed to efficiently forecast PV output power. This approach forecasts the short-term PV power depending on the distinctive model inputs such as historical meteorological factors and sub-power components. In this way, the relationship between the output and weather conditions is considered. The

framework of the deep forecasting method is illustrated in Fig. 4. The whole structure is composed of four main stages as the VMD method, data preprocessing and reconstruction of the inputs, training of the designed CNN model, and testing and evaluation of the network.

Firstly, the VMD is utilized to decompose the original PV output power and obtained the filtered series with different sub-frequencies. Let $P = \{p_{t-H+1}, p_{t-H+2}, \dots, p_t\}$ is the time-series original power data. Here, p_t is the sample at time t and H is the time horizon. With decomposing the data into five modes, the decomposed sub-power set can be derived as $\hat{P} = \{\text{IMF}_{1,t-H+1}, \text{IMF}_{2,t-H+2}, \dots, \text{IMF}_{m,t}\}$. Here m is mode level. While

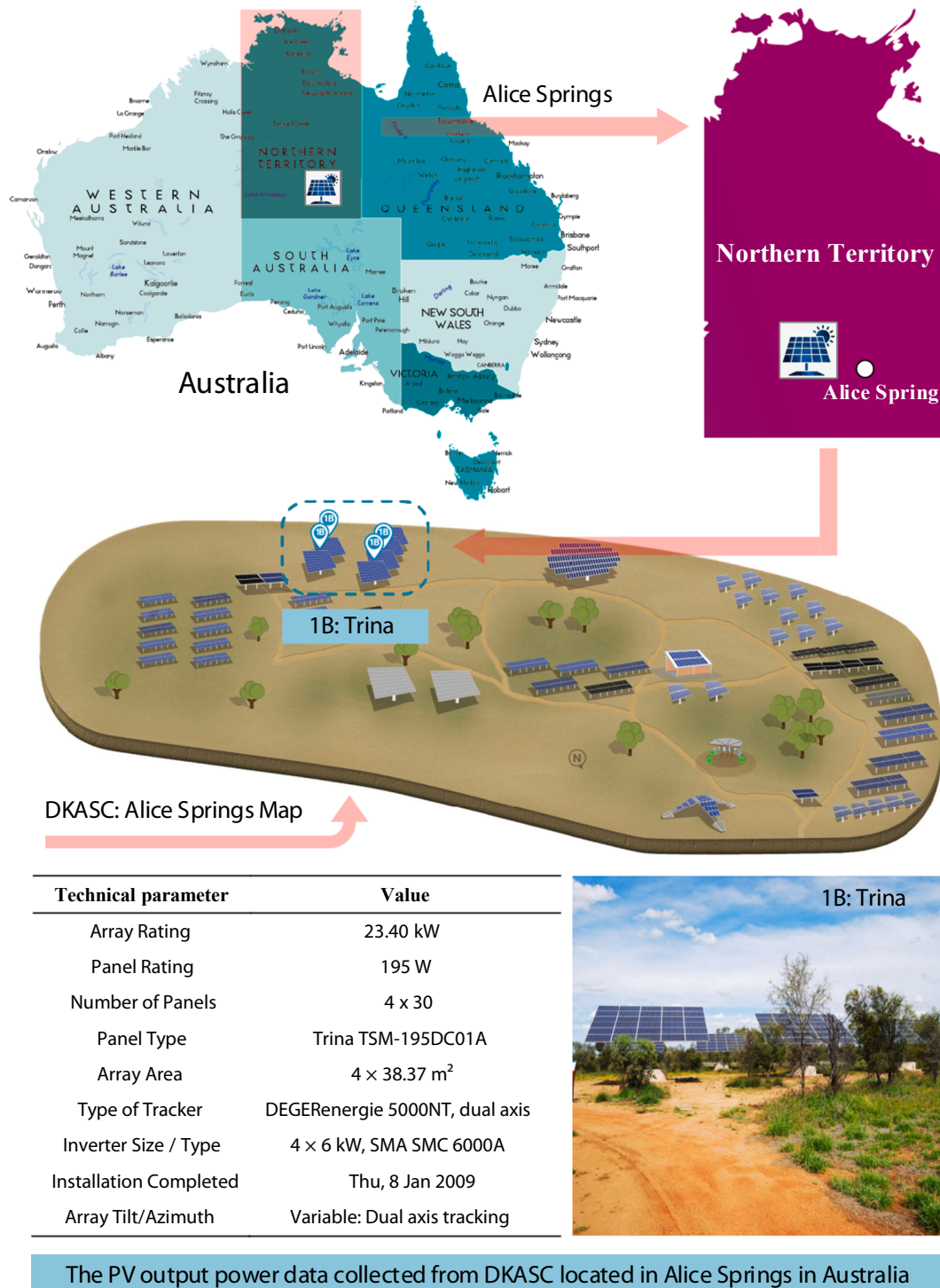


Fig. 5. General information and technical parameters of the dataset [44].

low-level frequencies define the trends of the output power, high-level frequencies define the rapid changes in the output.

Later, the time-series inputs are converted into 2D feature maps and concatenated into a single RGB image. This process constructs the new inputs with comprehensive daily and hourly correlations. After the reconstruction, all inputs and outputs are randomly divided for the training and validation subsets. The PV output power is also normalized to achieve better training performance. In the training stage, a parallel pooling-based CNN model is adopted as the deep learning forecasting unit. This architecture provides low computational cost and high forecasting accuracy.

During back-propagation, the stochastic gradient descent (SGD) algorithm is performed to optimize the whole cost function of the network. In this algorithm, the weights are updated for each iteration to get the goal rapidly [41] and the update rule is expressed as;

$$\Lambda_{t+1} = \Lambda_t - \eta_t \nabla H(\Lambda_t, B_t) \quad (14)$$

where η_t greater than 0 is the learning rate and $\nabla H(\Lambda_t, B_t)$ is the gradient of H on a mini-batch B_t . In addition, B_t can be given to approximate the inverse Hessian of G . The loss function of the network is selected as the RMSE. Finally, the well-trained network model is obtained and the testing data are used to evaluate the model performance. It is noted that the final forecasting results are transformed to the original scale in the evaluation.

4. Case study

In this section, the experimental studies and evaluations of the proposed deep forecasting method are presented in detail. All experiments are realized on a workstation with Intel (R) i7-10750H CPU @2.60 GHz, NVIDIA Quadro P620 GPU, and 16 GB RAM memory. The remainder of this section contains the dataset description, definitions of the benchmark networks, performance evaluation metrics, experimental results, analysis of the improvements, and comparison of the proposed method with state-of-the-art methods, respectively.

4.1. Dataset description

In this paper, the historical PV power data are collected from the Desert Knowledge Australia Solar Center (DKASC) located in Alice Springs in Australia. This data is a public dataset and can be openly accessed from [44]. Alice Springs is a solar rich city and covers 9% of the Northern Territory. The city climate can be classified in the Köppen as the desert climate with semi-arid conditions. The daily average temperature exceeds 30 °C for six months and the minimum average temperature is 5.5 °C in winter. In Alice Springs, a daily temperature changes up to 28 °C and the general climate structure is very convenient for PV systems [45].

The DKASC center includes Alice Springs, Yulara, and NT solar generating plants and Alice Springs is the most excellent plant with 38 sites. Therefore, the data is selected from No. 1B: Trina at Alice Springs in this study. The PV panels are mono-crystalline and the tracker system of the panels can adjust their orientations through the day. Fig. 5 shows the general information about the plant. The input parameters are selected as the historical temperature (°C), relative humidity (%), global horizontal radiation (Wh/m²), diffuse horizontal radiation (Wh/m²),

and decomposed IMFs (kW) while active power data (kW) is selected as the output. The weather conditions are available from the metering system. The dataset is collected between January 1th, 2017 to December 31th, 2019 periods and the data resolution is hourly intervals between 12 a.m. to 11p.m. for each day. Due to equipment breakdowns or maintenances, there are some missing data. After removing these missing values, there are 25,996 hourly samples in total. The statistical properties of the dataset are given in Table 2 corresponding to the minimum (Min), maximum (Max), median (Med), mean, standard deviation (Std), and percentiles (Pctl).

4.2. Benchmark networks

In order to verify the performance of the SolarNet, it is compared with the most well-known four pre-trained deep learning networks. In the comparisons, the following methods are considered: SqueezeNet, AlexNet, GoogLeNet, and ResNet-18 [46]. AlexNet is an effective CNN structure that includes 12 deep layers [41]. SqueezeNet is a smaller network with fewer learning parameters according to the AlexNet [47]. Contrary to the above networks, GoogLeNet and ResNet-18 are more complex networks with deeper layers. GoogLeNet has 22 deep layers and is a variant of the Inception network [48]. ResNet-18 is also an efficient CNN that is designed with residual connections. The above-mentioned CNNs are pre-trained networks on the ImageNet large-scale visual recognition challenge with more than one million images and have already learned to extract deep intrinsic features [41]. Therefore, they can be effectively utilized to perform new forecasting tasks by retraining.

4.3. Performance evaluation metrics

In order to evaluate the quantitative performance of the proposed method, three widely-used performance metrics are statistically used as correlation coefficient (R), RMSE, and mean absolute error (MAE). R gives the relationship between the outputs and targets. RMSE is the quadratic scoring rule that finds the standard deviation of the forecasting errors while MAE is the corresponding to the forecasted values of the absolute error losses. As each metric provides a specific evaluation opportunity, the obtained forecasting results can be proved in detail. These metrics can be given with the following equations:

$$R = \frac{1}{\sqrt{\sum_{i=1}^n (X_i - \bar{X})^2 \sum_{i=1}^n (Y_i - \bar{Y})^2}} \quad (15)$$

$$RMSE = \sqrt{\frac{1}{n} \sum_{i=1}^n (X_i - Y_i)^2} \quad (16)$$

$$MAE = \frac{1}{n} \sum_{i=1}^n |X_i - Y_i| \quad (17)$$

where X and \bar{X} are the observed and forecasted power values. Y and \bar{Y} are the mean of the observed and forecasted power samples. Therefore, the robustness and effectiveness abilities of the proposed method can be easily measured with the aforementioned metrics.

Table 2
Statistical properties of the dataset.

Parameter	M	Min	Max	Med	Mean	Std	Pctl (80)	Pctl (20)
Active Power (kW)	25,996	0	20.50	0.2132	4.03	5.21	9.13	0
Temperature (°C)	25,996	-4.66	45.23	22.28	21.96	9.96	31.09	12.98
Humidity (%)	25,996	3.01	102.38	26.73	31.99	20.65	48.50	13.86
Global Radiation (Wh/m ²)	25,996	0.35	1256.10	11.93	276.89	367.32	683.08	2.25
Diffuse Radiation (Wh/m ²)	25,996	0.40	624.64	8.57	49.64	78.96	80.51	1.22

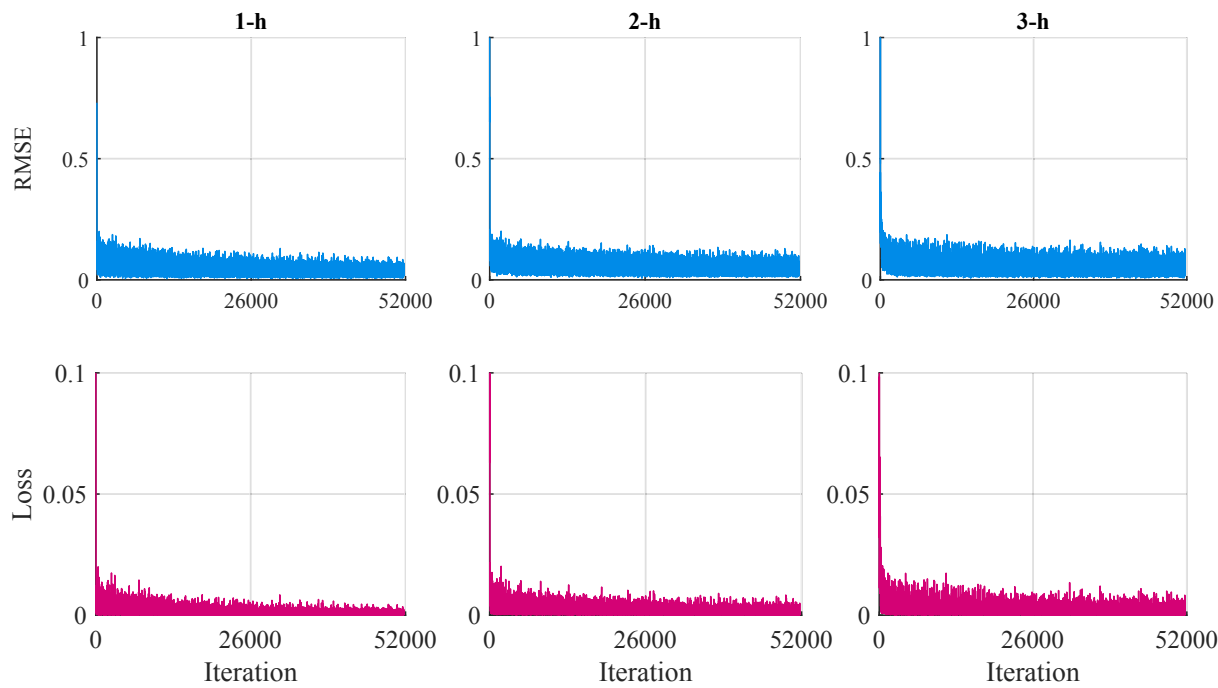


Fig. 6. Training processes of the parallel pooling structure-based SolarNet for 1-h to 3-h ahead.

4.4. Experimental studies

In the experiments, the historical dataset is from a manufacturer named Trina and the output power capacity of the PV system is 23.40 kW. It consists of active power with sub-components, temperature, humidity, global horizontal radiation, and diffuse horizontal radiation. After the reconstruction process, 25,870 samples are obtained for each data. 80% of the historical dataset is used for training while 10% is used for validation and 10% for testing. In the testing, the data from 2019 is only used. As is known, PV power is sensitive to seasonal changes and factors. The testing data are divided into four seasons as Winter (June-August), Spring (September-November), Summer (December-February), and Fall (March-May). In the training process, the mini-batch size and maximum epoch are given as 16 and 40, respectively. The learning rate is given as $1e-3$ and reduced by a drop factor of 0.5 after every 10 epochs (10: $5e-4$, 20: $2.5e-4$, and 30: $1.25e-4$). The comparisons are performed with the benchmark deep learning methods to verify the forecasting effectiveness of the SolarNet. The proposed network is also compared with the single pooling-based CNNs and the efficiency of the parallel pooling is verified. In the comparisons, actual data represents the PV power output of 1B: Trina.

Fig. 6 presents the training processes of the proposed CNN model for 1-h to 3-h ahead forecast horizons. The horizontal axis is the iteration number, and the vertical axis is the RMSE and loss values. In the training, 51,720 iterations are performed and the loss values are decreased to $5.266e-4$, $5.831e-4$, and $9.448e-4$, for 1-h ahead, 2-h ahead, and 3-h ahead, respectively.

Fig. 7 shows an example of the activations obtained from the convolutions of the network. *Conv-1*, *Conv-4-1*, *Conv-5-2*, and *Conv-6* represent the first convolution, last convolution of the parallel block 1, last convolution of the parallel block 2, and final convolution of the network, respectively. Therefore, it can be seen that which feature the network learns by comparing areas of activation with the original input image. In the figure, first 16 channels are given and the strongest activation channels for each convolution depending on the input are shown. While black pixels indicate strong negative activations, white pixels indicate strong positive activations. At some points, white pixels in a channel define the strongly activated channel at that position.

In order to analyze and evaluate the SolarNet, the experimental results of the parallel pooling structure are firstly compared to only max-pooling-based and only average-pooling-based CNN models. The rainy, cloudy, and sunny days are selected for testing data in 1-h to 3-h ahead

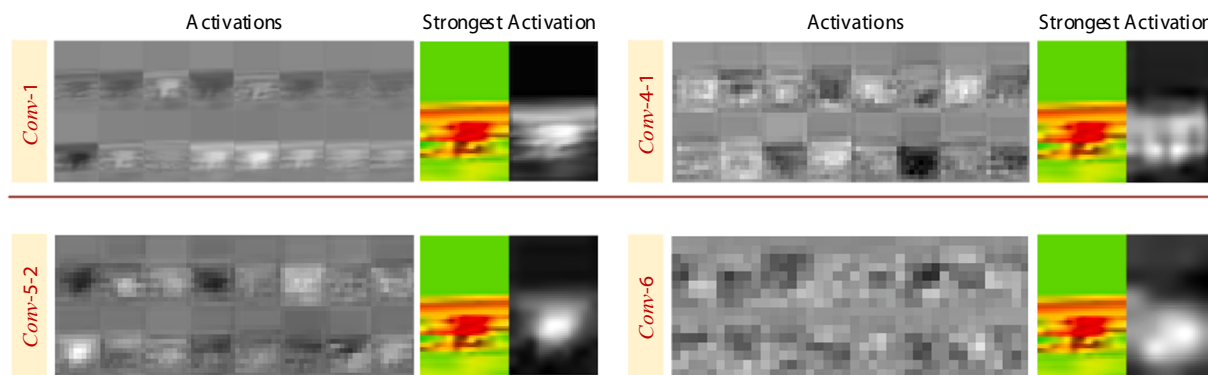


Fig. 7. An example of the activations obtained from the convolutions.

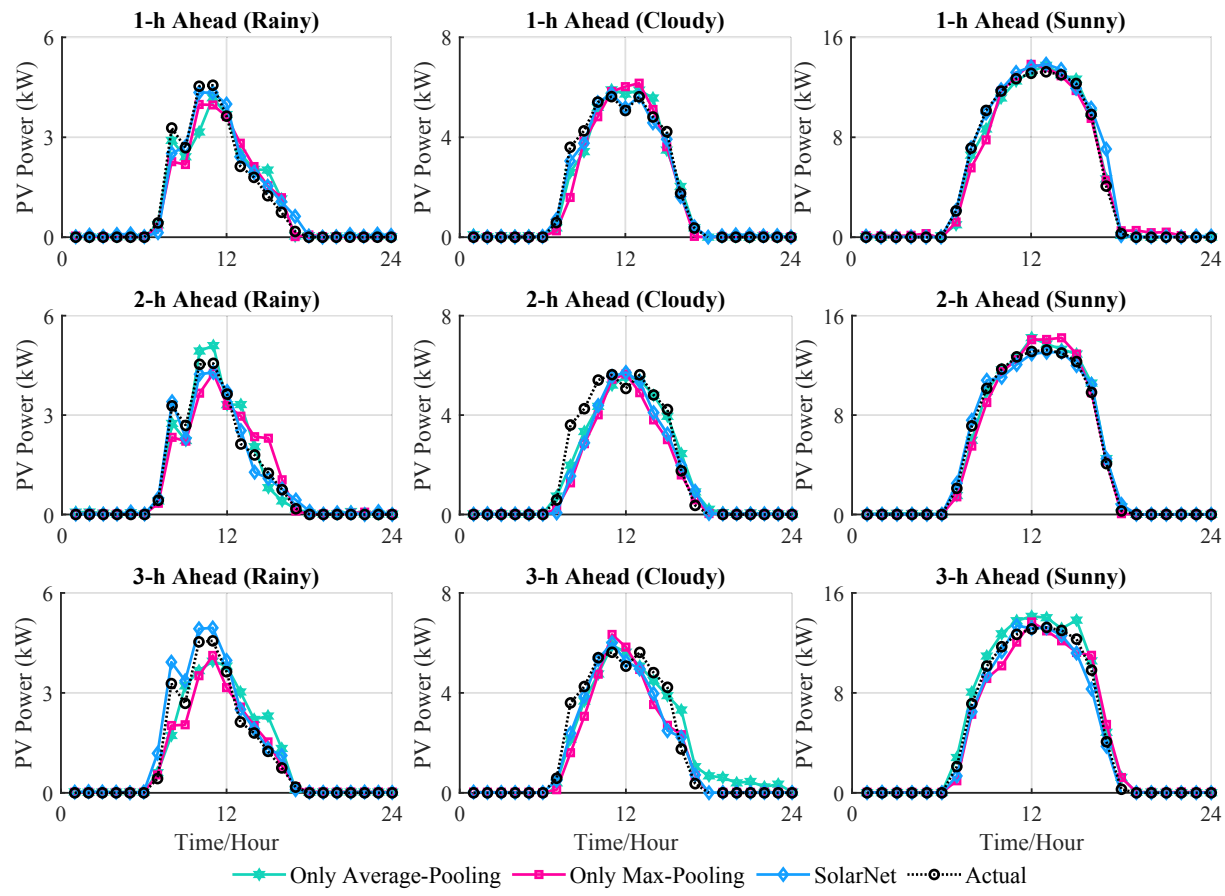


Fig. 8. Forecasting results of the pooling structures for different weather combinations.

Table 3

Forecasting results of the pooling structures for 1-h to 3-h forecast horizons.

Metrics	Horizon	Only Average-Pooling			Only Max-Pooling			SolarNet		
		Rainy	Cloudy	Sunny	Rainy	Cloudy	Sunny	Rainy	Cloudy	Sunny
R	1-h	0.9689	0.9715	0.9855	0.9706	0.9758	0.9878	0.9826	0.9873	0.9913
	2-h	0.9577	0.9581	0.9701	0.9612	0.9618	0.9752	0.9780	0.9788	0.9854
	3-h	0.9415	0.9504	0.9609	0.9501	0.9522	0.9656	0.9693	0.9702	0.9809
RMSE	1-h	0.3347	0.4309	0.3818	0.3046	0.4194	0.3643	0.2136	0.3878	0.3255
	2-h	0.3932	0.5380	0.4770	0.3707	0.5066	0.4565	0.2421	0.4574	0.4041
	3-h	0.4738	0.6834	0.5594	0.4465	0.6334	0.5377	0.2851	0.5485	0.4492
MAE	1-h	0.2182	0.2366	0.2835	0.2014	0.2143	0.2721	0.1465	0.1656	0.2128
	2-h	0.2701	0.4178	0.3394	0.2546	0.3581	0.3286	0.1647	0.2752	0.2472
	3-h	0.3211	0.4875	0.4124	0.3079	0.4396	0.3941	0.1870	0.3201	0.2903

forecast horizons. The weather conditions are determined from the testing data. As known, the PV power on rainy and cloudy days is quite difficult to forecast. The forecasting accuracy is relatively higher on sunny days. The forecasting results of each method are presented in Fig. 8. The obtained metric values are listed in Table 3. Moreover, Fig. 9 is given to better verify the forecasting effectiveness of the proposed method.

As can be seen from Table 3 and Fig. 9, the R values obtained from the SolarNet are calculated as 0.9826–0.9780–0.9693 for rainy days, 0.9873–0.9788–0.9702 for cloudy days, and 0.9913–0.9854–0.9809 for sunny days, which are better than those from the other methods. The forecasting performance of the SolarNet is better than that of the only max-pooling and only max-pooling methods in terms of RMSE values. For the proposed model, the RMSE values are 0.2136–0.2421–0.2851 on rainy days, 0.3878–0.4574–0.5485 on cloudy days, and 0.3255–0.4041–0.4492 on sunny days, respectively. Among the pooling

methods, only average-pooling has the worst results, whose values of RMSE are 0.3347–0.3932–0.4738 on rainy days, 0.4309–0.5380–0.6834 on cloudy days, and 0.3818–0.4770–0.5594 on sunny days, respectively. Similar to the R and RMSE values, the SolarNet provides the best forecasting results in terms of MAE values.

Subsequently, the performance and reliability of the proposed forecasting model are tested in all seasons to verify the forecasting reliability and effectiveness of the SolarNet. The forecasting studies are performed for all deep learning models. In these results, specific time intervals are zoomed to further analyze the accuracy of the obtained forecast results. In addition, the R, RMSE, and MAE values of all forecast methods are presented in Fig. 10 and Table 4. The forecasting results obtained from the season conditions are given in Figs. 11 to 13.

From the table and bar charts, it can be clearly observed that the SolarNet provides better forecasting results than benchmark methods for seasonal conditions. While the R values of the proposed method are

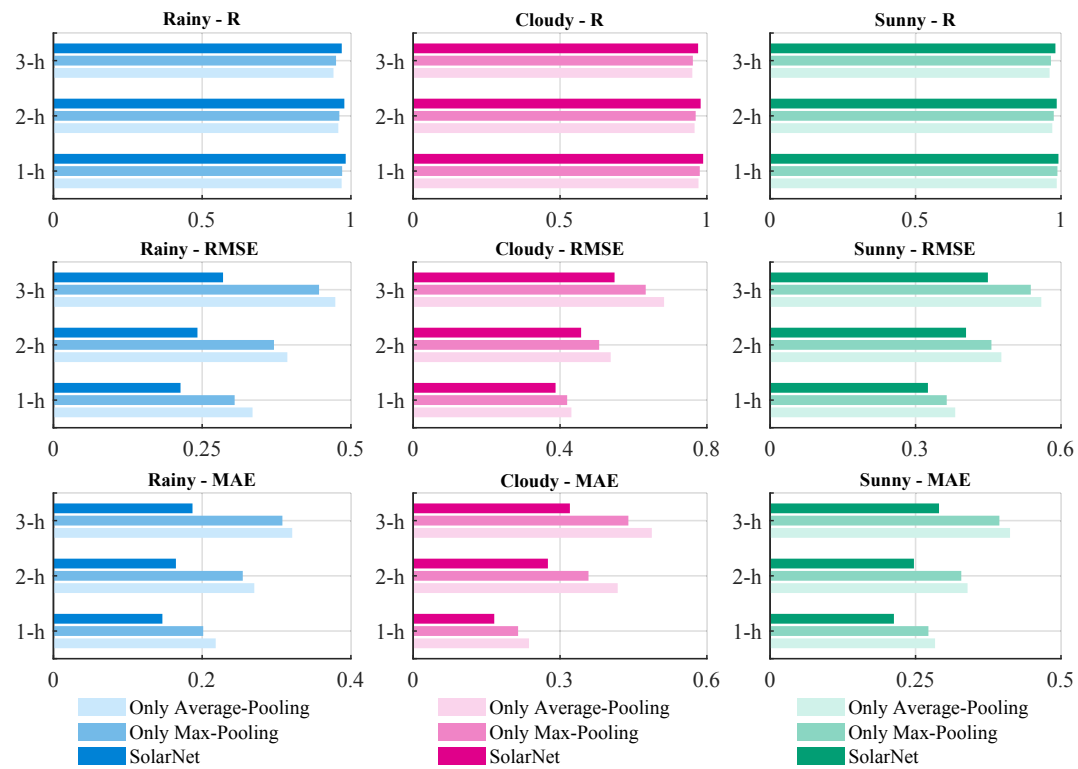


Fig. 9. Forecasting results of the pooling structures for 1-h to 3-h forecast horizons.

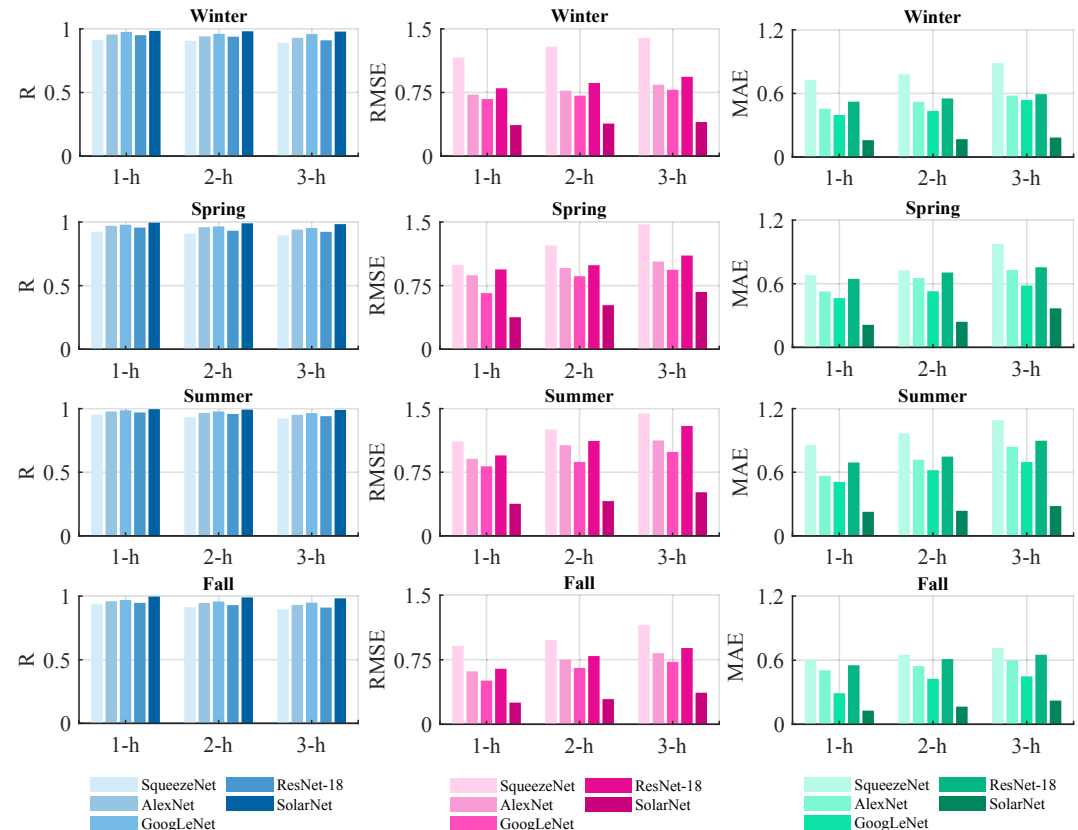


Fig. 10. Evaluation metrics of the different deep learning methods for each season.

Table 4

Forecasting performance of the different deep learning methods for each season.

Season	Method	R	RMSE			MAE		
		1-h	2-h	3-h	1-h	2-h	3-h	1-h
Winter	SqueezeNet	0.9136	0.9064	0.8905	1.1629	1.2890	1.3927	0.7250
	AlexNet	0.9565	0.9414	0.9301	0.7250	0.7708	0.8421	0.4558
	GoogLeNet	0.9764	0.9614	0.9585	0.6725	0.7123	0.7819	0.4353
	ResNet-18	0.9504	0.9388	0.9102	0.7997	0.8615	0.9346	0.5371
	SolarNet	0.9848	0.9811	0.9789	0.3656	0.3834	0.4016	0.1590
Spring	SqueezeNet	0.9244	0.9085	0.8954	0.9941	1.2233	1.4724	0.6816
	AlexNet	0.9702	0.9598	0.9410	0.8731	0.9585	1.0337	0.5275
	GoogLeNet	0.9789	0.9657	0.9536	0.9622	0.8610	0.9364	0.4645
	ResNet-18	0.9563	0.9318	0.9230	0.9409	0.9910	1.1052	0.6462
	SolarNet	0.9952	0.9901	0.9837	0.3777	0.5198	0.6755	0.2129
Summer	SqueezeNet	0.9534	0.9319	0.9230	1.1133	1.2533	1.4440	0.8580
	AlexNet	0.9775	0.9655	0.9510	0.9071	1.0687	1.1245	0.5657
	GoogLeNet	0.9870	0.9776	0.9650	0.8192	0.8711	0.9891	0.5090
	ResNet-18	0.9701	0.9579	0.9407	0.9483	1.1184	1.2955	0.6918
	SolarNet	0.9954	0.9920	0.9895	0.3783	0.4093	0.5136	0.2266
Fall	SqueezeNet	0.9401	0.9133	0.8961	0.9115	0.9785	1.1544	0.6028
	AlexNet	0.9601	0.9461	0.9302	0.6150	0.7502	0.8267	0.5059
	GoogLeNet	0.9697	0.9579	0.9489	0.5076	0.6549	0.7259	0.2908
	ResNet-18	0.9472	0.9294	0.9101	0.6452	0.7930	0.8862	0.5530
	SolarNet	0.9966	0.9901	0.9828	0.2521	0.2922	0.3670	0.1277

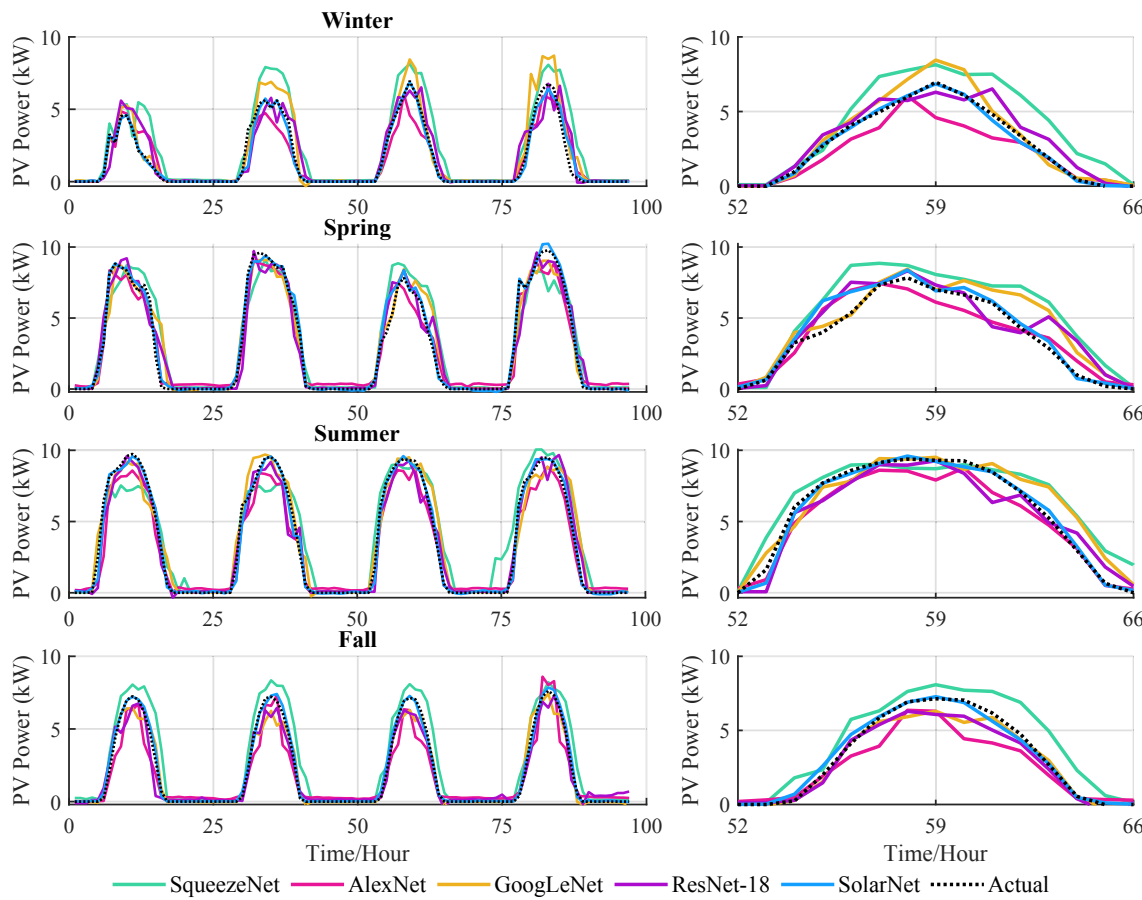


Fig. 11. Forecasting results for 1-h ahead under different seasons.

calculated as being 0.9848 for 1-h ahead, 0.9811 for 2-h ahead, and 0.9789 for 3-h ahead in Winter, the values of the SqueezeNet, AlexNet, GoogLeNet, and ResNet-18 are calculated as being 0.9136–0.9064–0.8905, 0.9565–0.9414–0.9301, 0.9764–0.9614–0.9585, and 0.9504–0.9388–0.9102, respectively. When the R values of all methods in Spring are compared, the values obtained from the SolarNet are 0.9952–0.9901–0.9837, which are smaller than those of

benchmark methods, i.e. 0.9244–0.9085–0.8954 from SqueezeNet, 0.9702–0.9598–0.9410 from AlexNet, 0.9789–0.9657–0.9536 from GoogLeNet, and 0.9563–0.9318–0.9230 from ResNet-18. The obtained results indicate that the proposed method significantly increases the forecast accuracy. From the comparison of all forecasting methods for Summer and Fall seasons, it can be seen that the SolarNet has the best R values, followed by the GoogLeNet, then is the AlexNet, and SqueezeNet

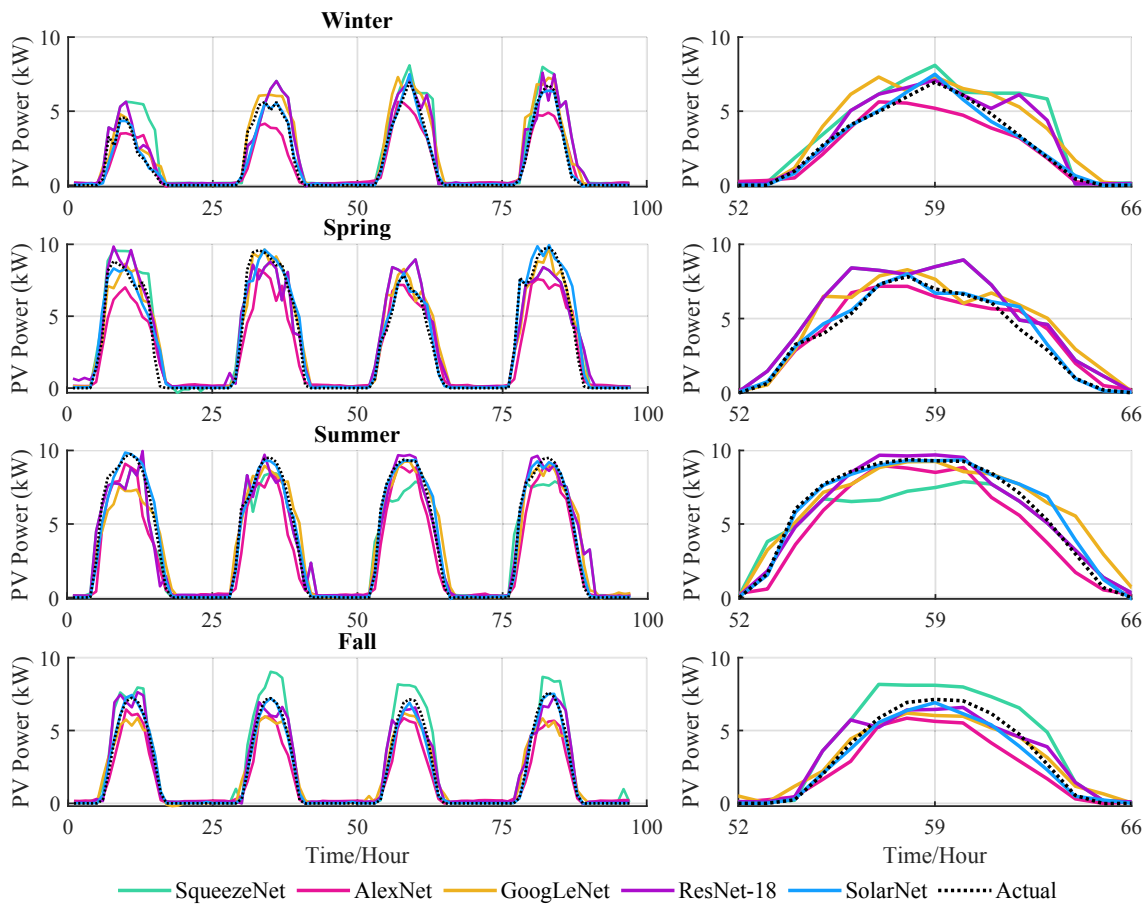


Fig. 12. Forecasting results for 2-h ahead under different seasons.

has the worst values. For instance, the R values of proposed method, SqueezeNet, AlexNet, GoogLeNet, and ResNet-18 are 0.9954–0.9534–0.9775–0.9870–0.9701 for 1-h ahead, 0.9920–0.9319–0.9655–0.9776–0.9579 for 2-h ahead and 0.9895–0.9230–0.9510–0.9650–0.9407, respectively in Summer. Specifically, the comparison studies are confirmed that the proposed method guarantees more reliable forecasting results.

When the RMSE values obtained from all seasons are analyzed, the following evaluations can be reached from Figs. 10 to 13 and Table 4. In Winter, the RMSE values of the SolarNet are 0.3656 for 1-h ahead, 0.3834 for 2-h ahead, and 0.4016 for 3-h ahead, indicating that the proposed model provides more accurate forecasting results than those of the benchmark methods. GoogLeNet has the second best RMSE results for the winter season, which is 0.6725 for 1-h ahead, 0.7123 for 2-h ahead, 0.7819 for 3-h ahead, respectively. Despite the increase in the forecast horizon, the forecasting results from the proposed method are more stable compared to benchmark methods. From RMSE values in Spring and Summer, it can be seen that the SolarNet is superior to the other methods. For instance, the RMSE values of the SolarNet are calculated as being 0.3777 to 0.3783 for 1-h ahead, 0.5198 to 0.4093 for 2-h ahead, and 0.6755 to 0.5136 for 3-h ahead, respectively whilst the calculated RMSE values of GoogLeNet are 0.9622 to 0.8192 for 1-h ahead, 0.8610 to 0.8711 for 2-h ahead, 0.9364 to 0.9891 for 1-h ahead, respectively. These values guarantee that the proposed method is not only superior to other methods, but also provides higher forecasting accuracy and capability. From Fall, the RMSE values of the proposed method are calculated as 0.2521 for 1-h ahead, 0.2922 for 2-h ahead, and 0.3670 for 3-h ahead, respectively. The closest to the results of the proposed method is GoogLeNet, which are 0.5076 for 1-h ahead, 0.6549 for 2-h ahead, and 0.7259 for 3-h ahead, respectively.

SqueezeNet has the worst forecasting results amongst all methods, which are 0.9115 for 1-h ahead, 0.9785 for 2-h ahead, 1.1544 for 3-h ahead, respectively. Considering all the calculated RMSE values, the proposed method has the lowest values, which is significant proof that it improves forecast accuracy.

The forecasting results of the proposed method are compared with those of other state-of-the-art models in terms of their MAE values. The following evaluations can be summarized from Figs. 10 to 13 and Table 4. The MAE values of the SolarNet for Winter are computed as 0.1590 for 1-h ahead, 0.1683 for 2-h ahead, and 0.1837 for 3-h ahead, respectively. The MAE values of GoogLeNet are the second-best compared to other methods, while SqueezeNet shows the poorest results, which are 0.7250 for 1-h ahead, 0.7801 for 2-h ahead, and 0.8863 for 3-h ahead, respectively. Despite the increase in the forecast horizon, the MAE values of the proposed method slightly change over other methods. The MAE values of the SolarNet in Spring and Summer are calculated as 0.2129 to 0.2266 for 1-h ahead, 0.2415 to 0.2363 for 2-h ahead, and 0.3683 to 0.2808 for 3-h ahead, respectively. Similar to other evaluation metric results, it is observed that GoogLeNet has the second-best results, which are 0.4645 to 0.5090 for 1-h ahead, 0.5297 to 0.6195 for 2-h ahead, and 0.5839 to 0.6956 for 3-h ahead, respectively.

These metric values clearly show that more accurate and reliable forecasting results can be obtained with the proposed method. When the MAE values in Fall are analyzed, the proposed method has the best values compared to the other methods. For example, the MAE values of the SolarNet are calculated as 0.1277 for 1-h ahead, 0.1652 for 2-h ahead, and 0.2219 for 3-h ahead, whilst those of GoogLeNet, which has the second-best values, are 0.2908 for 1-h ahead, 0.4258 for 2-h ahead, and 0.4489 for 3-h ahead, respectively. SqueezeNet shows the worst results, which are 0.6028 for 1-h ahead, 0.6495 for 2-h ahead, and

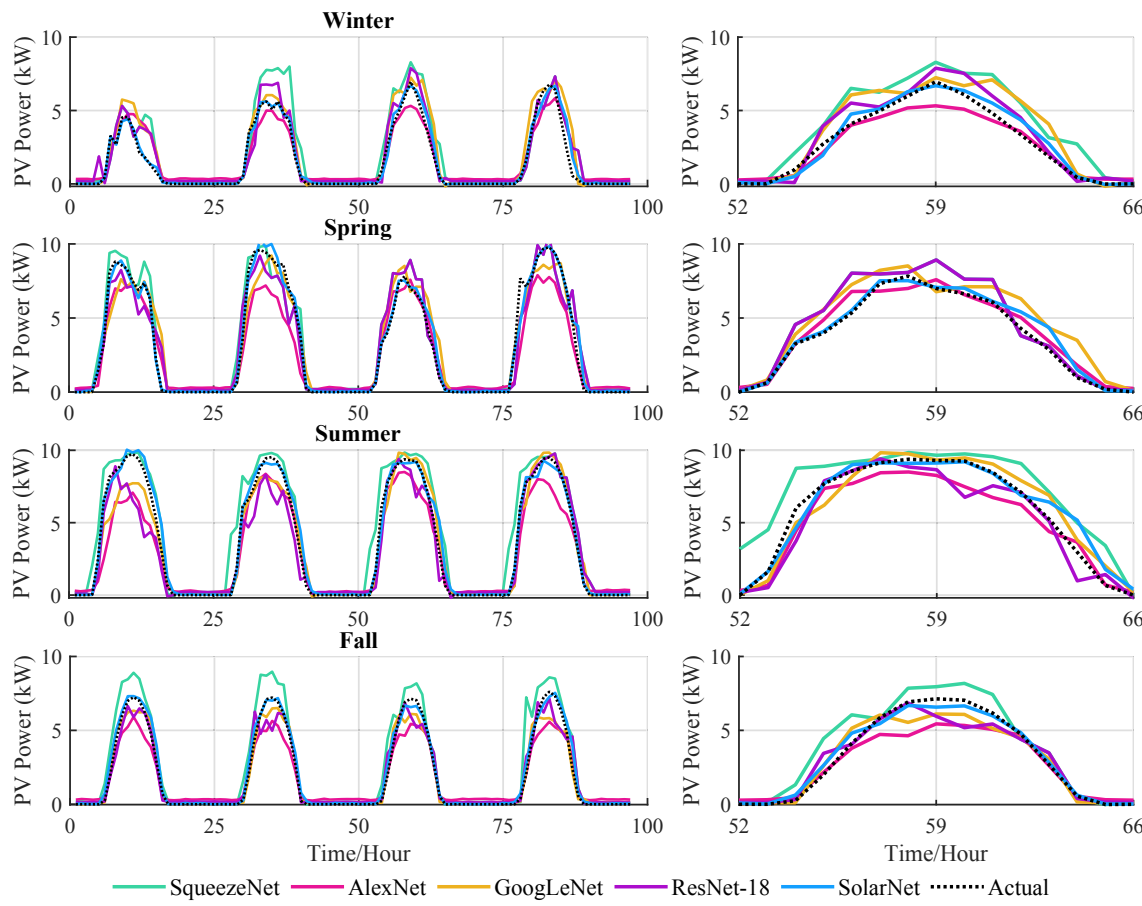


Fig. 13. Forecasting results for 3-h ahead under different seasons.

Table 5
Monthly forecasting results of the SolarNet for 2019.

Horizon	Metric	Jan.	Feb.	Mar.	Apr.	May.	Jun.	Jul.	Aug.	Sep.	Oct.	Nov.	Dec.
1-h	R	0.9841	0.9829	0.9852	0.9837	0.9855	0.9895	0.9898	0.9895	0.9891	0.9823	0.9849	0.9828
	RMSE	0.7265	0.7528	0.6744	0.6719	0.4988	0.3802	0.4022	0.4595	0.5205	0.7147	0.7968	0.6647
	MAE	0.4026	0.4253	0.3964	0.3640	0.2778	0.2265	0.2380	0.2632	0.3136	0.4199	0.4650	0.3998
2-h	R	0.9813	0.9827	0.9837	0.9805	0.9811	0.9867	0.9868	0.9881	0.9848	0.9742	0.9776	0.9791
	RMSE	0.8065	0.7906	0.7079	0.7394	0.5503	0.4241	0.4436	0.4809	0.6057	0.9045	0.9084	0.7499
	MAE	0.4982	0.4626	0.4447	0.4472	0.3628	0.2825	0.3094	0.3244	0.4019	0.5816	0.5877	0.4669
3-h	R	0.9802	0.9796	0.9852	0.9784	0.9737	0.9849	0.9841	0.9813	0.9761	0.9674	0.9683	0.9742
	RMSE	0.8578	0.8420	0.7714	0.7673	0.7569	0.4558	0.4859	0.7840	0.7826	0.9697	0.9677	0.8380
	MAE	0.5194	0.4965	0.4965	0.4552	0.4608	0.3246	0.3586	0.4909	0.4884	0.6434	0.6258	0.5049

0.7146 for 3-h ahead, respectively. Despite the difficult seasonal conditions and the increasing forecast horizon, the proposed method is proven to guarantee more reliable and accurate forecasting results.

Moreover, monthly values of R, RMSE, and MAE are calculated to investigate the forecast performance of the proposed method in more detail. The monthly forecasting results obtained from the proposed method are given in Table 5. In addition, radar graphs for each metric are presented in Fig. 14 to better evaluate the obtained results. The average values of R are calculated as being 0.9858 for 1-h ahead, 0.9811 for 2-h ahead, and 0.9765 for 3-h ahead, respectively. The average values of RMSE values change from 0.6053 to 0.7743. The average values of MAE are 0.3493 for 1-h ahead, 0.4308 for 2-h ahead, and 0.4896 for 3-h ahead, respectively. The obtained metric values are at very satisfactory levels as expected. From metric results, it can be clearly stated that the proposed method provides high forecast accuracy.

Table 6 presents the comparison of the networks to show the complexity and easily applicable for the embedded systems. While the

AlexNet gives the highest learnable parameter, the SolarNet has the lowest. In addition, the number of learnable parameters of the designed CNN is 2 times less than the network with the second-lowest parameter.

4.5. Analysis of improvement percentages for the pooling structures

The improvement percentages are statistically obtained to prove the effectiveness and stability of the parallel pooling structure over only average-pooling and only max-pooling. The improvement percentages of the only average-pooling and the only max-pooling structures are given in Table 7. This table indicates that the proposed model has not only more accurate forecasting ability than other structures but also significantly guarantees more reliable forecasting results. More specifically, the following assessments can be expressed in Fig. 15. The proposed method outperforms consistently the other pooling structures in terms of R, RMSE, and MAE in all forecast horizons. From the 1-h to 3-h ahead forecasting results of rainy, cloudy, and sunny days, the

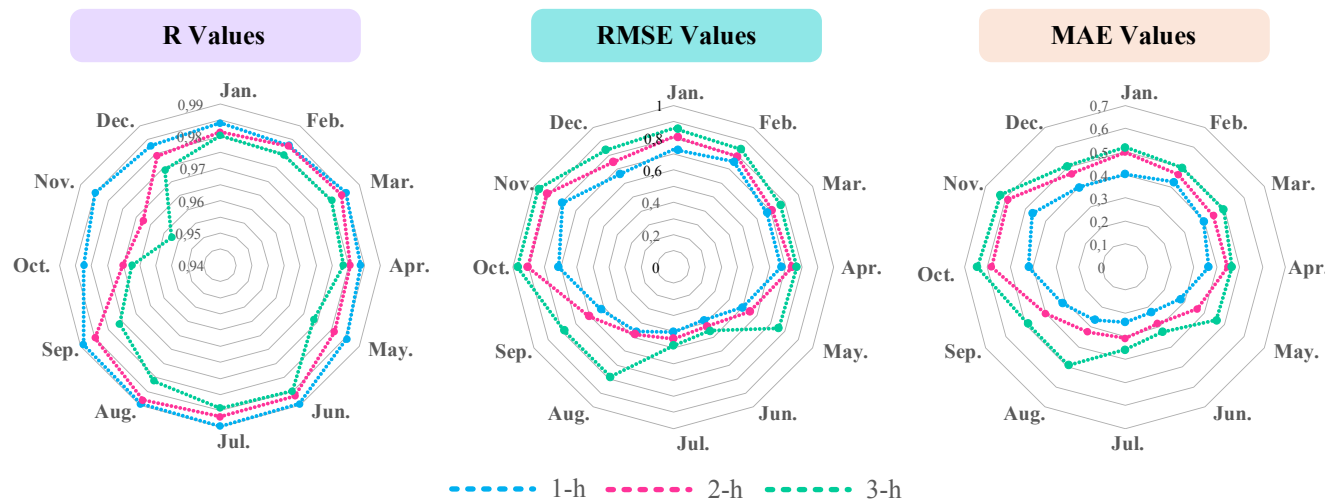


Fig. 14. Radar charts of the monthly metrics for 2019.

Table 6

Comparison of learnable parameters. It is noted that K and M represent 10^3 and 10^6 multipliers.

Criteria	Networks				
	SqueezeNet	AlexNet	GoogLeNet	ResNet-18	SolarNet
Learnable Parameters (~)	1.2 M	60.9 M	2.4 M	11.1 M	600 K

improvements in R values of the only average-pooling are 1.414%-1.626%-0.588% for 1-h ahead, 2.119%-2.160%-1.577% for 2-h ahead, and 2.421%-2.083%-2.081% for 3-h ahead, respectively. The improvement percentages in R values for the only max-pooling are calculated as 1.236%-1.178%-0.354% for 1-h ahead, 1.747%-1.767%-1.045% for 2-h ahead, and 2.021%-1.890%-1.584% for 3-h ahead, respectively.

Comparing the proposed method with the only average-pooling, the improvement percentages of RMSE values for rainy, cloudy, and sunny days are calculated as being 29.88%-7.53%-10.65 for 1-h ahead, 38.42%-14.98%-15.28% for 2-h ahead, and 39.82%-19.74%-19.70% for 3-h ahead, respectively. When compared the parallel pooling with the only max-pooling, the parallel structure improves the RMSE values by 15.68%-11.79%-15.49% for 1-h ahead, 34.69%-9.72%-11.48% for 2-h ahead, and 36.14%-13.40%-16.46% for 3-h ahead, respectively. These values prove that the parallel pooling structure is a reliable and powerful model and the parallel pooling structure increases the forecasting performance. The improvement percentages in MAE values of the parallel pooling over that of the only average-pooling method for rainy, cloudy, and sunny days are calculated as 32.86%-30.01%-24.94% for 1-h ahead, 39.02%-23.15%-24.77% for 2-h ahead, and 41.76%-34.34%-29.61% for 3-h ahead, respectively. While those of the only max-pooling are 27.26%-22.73%-21.79% for 1-h ahead, 35.31%-23.15%-24.77% for 2-h

ahead, and 39.27%-27.18%-26.34% for 3-h ahead, respectively. The obtained results clearly verify that the parallel pooling provides satisfactory forecast accuracy. Among the pooling structures, only max-pooling is provided the closest results to the parallel pooling.

4.6. Comparison between the proposed method and state-of-the-art methods

In this paper, the historical data are collected from the DKASC located in Australia and it is a publicly accessed dataset. In the existing studies, various state-of-the-art methods were performed and analyzed with solar generating plants from the DKASC. Therefore, a general performance comparison is given with these methods, as shown in Table 8.

According to Table 8, Zang et al. [3] proposed a day-ahead PV power forecasting approach based on deep learning models. ResNet and DenseNet models were introduced as the core models. A data preprocessing was given to construct input feature maps and a meta-learning strategy was proposed. They used the data from Nov. 11th, 2008 to Dec. 24th, 2018 with a 1-h resolution. Their forecasting approach reached the MAE values of rainy, cloudy, and sunny days as 0.3500, 0.2340, and 0.0850, respectively. While the minimum MAE of sunny days was reached with this study, the cloudy and rainy days gave higher MAE values. Chen et al. [6] also proposed a radiation classification coordinate (RCC) method to classify and select similar time periods. Based on the characteristics of PV power, the selected similar time period dataset was reconstructed as the training subset and the LSTM model was applied as the learning network. The dataset was collected from the Yulara in Alice Springs for two (2017 and 2018) years. They obtained the average RMSE and MAE values for all seasons as 0.9400 and 0.5870, respectively. Wang et al. [7] designed a CNN, LSTM, and hybrid CNN-LSTM (CLSTM), and applied to the collected data in DKASC, 1B, Alice Springs PV system. The data were selected in 2014–2017 years with a 5-min resolution. Their average

Table 7

Improvement percentage of the pooling structures by the parallel pooling structure-based SolarNet.

Condition	Method	R (%)			RMSE (%)			MAE (%)		
		1-h	2-h	3-h	1-h	2-h	3-h	1-h	2-h	3-h
Rainy Day	Only Average-Pooling	1.414	2.119	2.421	36.18	38.42	39.82	32.86	39.02	41.76
	Only Max-Pooling	1.236	1.747	2.021	29.88	34.69	36.14	27.26	35.31	39.27
Cloudy Day	Only Average-Pooling	1.626	2.160	2.083	10.01	14.98	19.74	30.01	32.52	34.34
	Only Max-Pooling	1.178	1.767	1.890	7.53	9.72	13.40	22.73	23.15	27.18
Sunny Day	Only Average-Pooling	0.588	1.577	2.081	14.75	15.28	19.70	24.94	27.17	29.61
	Only Max-Pooling	0.354	1.045	1.584	10.65	11.48	16.46	21.79	24.77	26.34

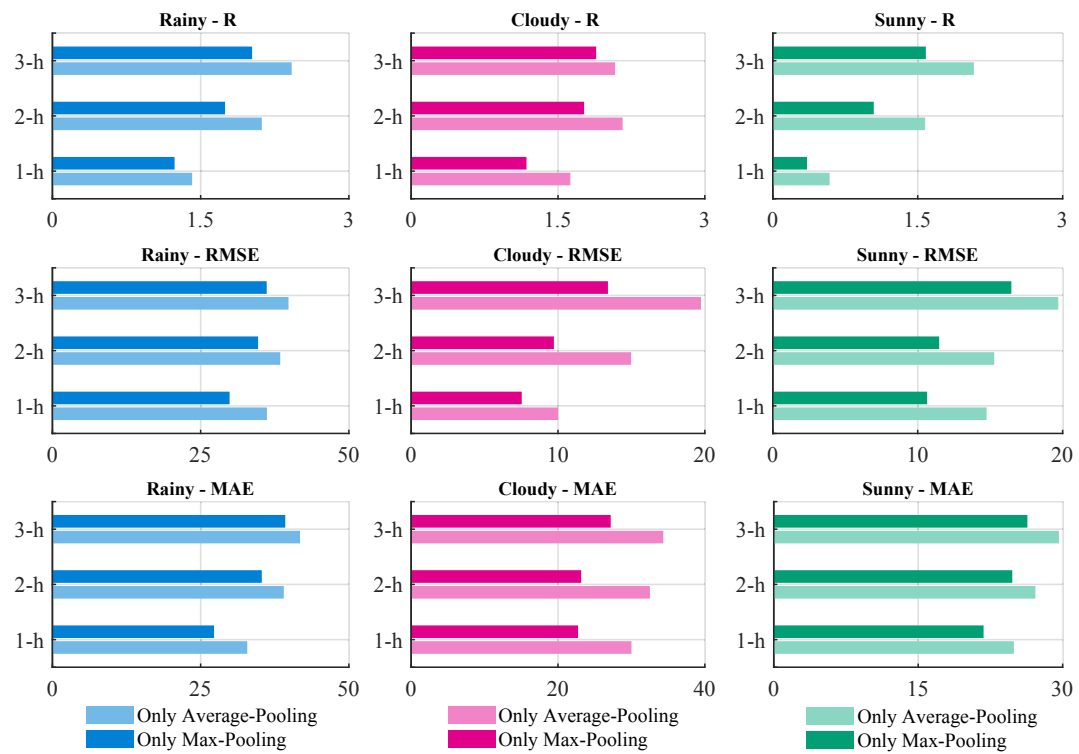


Fig. 15. Improvement percentages of the only max-pooling and only average-pooling structures by the proposed parallel pooling structure-based SolarNet.

Table 8

General comparison of the proposed SolarNet with some state-of-the-art methods.

Study	Year	Method	Dataset	Active Power	Date	Resolution	Forecast Horizon	Forecast Condition	RMSE	MAE
Zang et al. [3]	2020	DenseNet	DKASC, Alice Springs,	5.00 kW	Nov. 11, 2008-Dec. 24, 2018	1 h	–	Rainy Cloudy Sunny	– – 0.0850	0.3500 0.2340 0.2119
Chen et al. [6]	2020	RCC-LSTM	DKASC, Yulara, 3A	22.56 kW	2017–2018	5 min	–	–	0.9400	0.5870
Wang et al. [7]	2019	CLSTM	DKASC, Alice Springs, 1B	23.40 kW	2014–2017	5 min	–	–	0.3430	0.1260
Li et al. [18]	2019	HIMVO-SVM	DKASC, Alice Springs	–	Jan.–Aug., 2017	30 min	–	Rainy Cloudy Sunny	– – 0.2119	0.2888 0.3409 0.2119
Zhou et al. [24]	2020	SDA-GA-ELM	DKASC	4.95 kW	Jan. 14, 2017-Oct. 15, 2018	1 h	–	–	–	0.2367
Wang et al. [34]	2019	LSTM-CNN	DKASC, Alice Springs, 1B	23.40 kW	–	5 min	5 min	–	0.6210	0.2210
Present Study	2021	SolarNet	DKACS, Alice Springs, 1B	23.40 kW	2017–2019	1 h	1 h	Rainy Cloudy Sunny Average	0.2136 0.3878 0.3255 0.3090	0.1465 0.1656 0.2128 0.1750

RMSE and MAE are 0.3430 and 0.1260, respectively, but the forecast cases were not indicated. While the average MAE is the lowest, the obtained RMSE value is higher in this study. Li et al. [18] designed a hybrid improved multi-verse optimizer algorithm (HIMVO) to optimize the support vector machine (SVM) model and proposed HIMVO-SVM forecasting model. The dataset was selected from DKASC between Jan. to Oct., 2017 with 30-min resolution. Their method was evaluated for different weather conditions and they reached the MAE values of rainy, cloudy, and sunny days as 0.2888, 0.3409, and 0.2119, respectively. Zhou et al. [24] proposed a hybrid forecasting model namely SDA-GA-ELM based on ELM, genetic algorithm (GA) and customized similar day analysis (SDA). In the SDA, the Pearson correlation coefficient was employed to measure the similarity between different days based on meteorological factors, and the data samples similar to those from the

target forecast day were selected as the training set of ELM. The dataset was employed from Jan. 14, 2017 to Oct. 15, 2018 with a resolution of 1-h. Their method reached a higher MAE value of 0.2367. Wang et al. [34] presented a hybrid LSTM-CNN deep learning model. Their method extracted the temporal features of the data with the LSTM and the spatial features were extracted with the designed CNN model. The 1B DKASC, Alice Springs PV system data was selected with a 5-min resolution. The average RMSE and MAE values were obtained as 0.6210 and 0.2210, respectively.

When the results of the above studies are examined, the proposed SolarNet achieves the lowest MAE values for rainy and cloudy days. In addition, the proposed method gives the lowest average RMSE and MAE values for different weather conditions. Although the literature studies commonly selected the data resolution as 5-min, this study is

determined as a 1-h resolution and achieves higher forecasting performances. It can be clearly seen that the proposed method outperforms similar studies and presents the superior performance for PV output forecasting. As a result, this study not only proposes a novel and efficient PV power forecasting approach but also validates the SolarNet with different weather conditions and all seasons.

5. Conclusion

The use of solar energy is one of the RESs, which has become quite common in recent years. Accurate and reliable forecasting of PV power provides significant decision support for the planning and operation of power systems. In this study, a novel and effective CNN architecture-based (SolarNet) PV power forecasting method is proposed to forecast 1-h to 3-h ahead of solar power. The developed CNN model utilizes two parallel blocks as max-pooling and average-pooling to improve the generalized forecasting performance. The framework of the whole method includes the VMD method, data preprocessing, reconstruction of the feature maps, training of the CNN model, and decision-making mechanism. The VMD method decomposes the historical power data into sub-components and all of the input data are converted to 2D input images. Afterward, all time-series data are converted to HSV color space and concatenated into a single RGB image to feed the input of the network. In the parallel blocks, max-pooling and average-pooling layers with convolutions are utilized and the multiscale deep features with different levels of visual perception can be achieved. Finally, the designed parallel pooling structure forecasts the PV output power by extracting all intrinsic deep features.

All experiments are realized in three main cases including sunny, cloudy, and rainy days, all seasons, and monthly forecasting. The SolarNet is also evaluated with the single pooling structures and the obtained results are compared with the benchmark deep learning methods to evaluate the effectiveness of the designed CNN model. For all weather conditions, the proposed method reaches the highest R values. The average R values are achieved as 0.9871, 0.9807, and 0.9735 for 1-h, 2-h, and 3-h forecast horizons, respectively. The proposed method also gives the lowest average RMSE values as 0.3090, 0.3679, and 0.4276 for 1-h, 2-h, and 3-h forecast horizons, respectively. For 1-h to 3-h forecast horizons, the average R values of all seasons are obtained as 0.9930, 0.9883, and 0.9837 while the average RMSE values are achieved as 0.3434, 0.4012, 0.4894, respectively. Similar to the average R and RMSE values, the SolarNet provides the best forecasting results in terms of MAE values. Considering the designed CNN architecture, the parallel pooling structure increases the accuracy and exhibits superior performance in both single pooling structures and most-known deep learning methods. The experimental results indicate that the proposed deep forecasting method has more accurate and reliable prediction responses than other models in all test points. When all results are taken into account, it can be clearly stated that the SolarNet can provide more acceptable forecasting responses, as well as more effective planning of power systems.

In future works, the proposed method can be improved with various optimization algorithms. In addition, more nonlinear weather conditions and sun situation images can be added to the designed forecasting architectures to increase the forecasting accuracy.

CRediT authorship contribution statement

Deniz Korkmaz: Conceptualization, Data curation, Formal analysis, Investigation, Methodology, Software, Validation, Visualization, Writing – original draft, Writing - review & editing.

Declaration of Competing Interest

The authors declare that they have no known competing financial interests or personal relationships that could have appeared to influence

the work reported in this paper.

References

- [1] Sobri S, Koohi-Kamali S, Rahim NA. Solar photovoltaic generation forecasting methods: A review. *Energy Convers Manag* 2018;156:459–97. <https://doi.org/10.1016/j.enconman.2017.11.019>.
- [2] Abdel-Nasser M, Mahmoud K. Accurate photovoltaic power forecasting models using deep LSTM-RNN. *Neural Comput Appl* 2019;31:2727–40. <https://doi.org/10.1007/s00521-017-3225-z>.
- [3] Zang H, Cheng L, Ding T, Cheung KW, Wei Z, Sun G. Day-ahead photovoltaic power forecasting approach based on deep convolutional neural networks and meta learning. *Int J Electr Power Energy Syst* 2020;118:105790. <https://doi.org/10.1016/j.ijepes.2019.105790>.
- [4] Das UK, Tey KS, Seyedmahmoudian M, Mekhilef S, Idris MYI, Van Deventer W, et al. Forecasting of photovoltaic power generation and model optimization: A review. *Renew Sustain Energy Rev* 2018;81:912–28. <https://doi.org/10.1016/j.rser.2017.08.017>.
- [5] Yildiz C, Acikgoz H. A kernel extreme learning machine-based neural network to forecast very short-term power output of an on-grid photovoltaic power plant. *Energy Sources, Part A Recover Util Environ Eff* 2020;43:395–412. <https://doi.org/10.1080/15567036.2020.1801899>.
- [6] Chen B, Lin P, Lai Y, Cheng S, Chen Z, Wu L. Very-Short-Term Power Prediction for PV Power Plants Using a Simple and Effective RCC-LSTM Model Based on Short Term Multivariate Historical Datasets. *Electronics* 2020;9:289.
- [7] Wang K, Qi X, Liu H. A comparison of day-ahead photovoltaic power forecasting models based on deep learning neural network. *Appl Energy* 2019;251:113315. <https://doi.org/10.1016/j.apenergy.2019.113315>.
- [8] Wang H, Yi H, Peng J, Wang G, Liu Y, Jiang H, et al. Deterministic and probabilistic forecasting of photovoltaic power based on deep convolutional neural network. *Energy Convers Manag* 2017;153:409–22. <https://doi.org/10.1016/j.enconman.2017.10.008>.
- [9] Wang F, Xuan Z, Zhen Z, Li K, Wang T, Shi M. A day-ahead PV power forecasting method based on LSTM-RNN model and time correlation modification under partial daily pattern prediction framework. *Energy Convers Manag* 2020;212:112766. <https://doi.org/10.1016/j.enconman.2020.112766>.
- [10] Pan M, Li C, Gao R, Huang Y, You H, Gu T, et al. Photovoltaic power forecasting based on a support vector machine with improved ant colony optimization. *J Clean Prod* 2020;277:123948. <https://doi.org/10.1016/j.jclepro.2020.123948>.
- [11] Lima MAFB, Carvalho PCM, Fernández-Ramírez LM, Braga APS. Improving solar forecasting using Deep Learning and Portfolio Theory integration. *Energy* 2020;195. <https://doi.org/10.1016/j.energy.2020.117016>.
- [12] Almonacid F, Pérez-Higueras PJ, Fernández EF, Hontoria L. A methodology based on dynamic artificial neural network for short-term forecasting of the power output of a PV generator. *Energy Convers Manag* 2014;85:389–98. <https://doi.org/10.1016/j.enconman.2014.05.090>.
- [13] Ahmad MW, Moursched M, Rezgui Y. Tree-based ensemble methods for predicting PV power generation and their comparison with support vector regression. *Energy* 2018;164:465–74. <https://doi.org/10.1016/j.energy.2018.08.207>.
- [14] Chu Y, Urquhart B, Gohari SMI, Pedro HTC, Kleissl J, Coimbra CFM. Short-term reforecasting of power output from a 48 MWe solar PV plant. *Sol Energy* 2015;112:68–77. <https://doi.org/10.1016/j.solener.2014.11.017>.
- [15] Kushwaha V, Pindoriya NM. A SARIMA-RVFL hybrid model assisted by wavelet decomposition for very short-term solar PV power generation forecast. *Renew Energy* 2019;140:124–39. <https://doi.org/10.1016/j.renene.2019.03.020>.
- [16] Akhter MN, Mekhilef S, Mokhlis H, Shah NM. Review on forecasting of photovoltaic power generation based on machine learning and metaheuristic techniques. *IET Renew Power Gener* 2019;13:1009–23. <https://doi.org/10.1049/iet-rpg.2018.5649>.
- [17] Eseye AT, Zhang J, Zheng D. Short-term photovoltaic solar power forecasting using a hybrid Wavelet-PSO-SVM model based on SCADA and Meteorological information. *Renew Energy* 2018;118:357–67. <https://doi.org/10.1016/j.renene.2017.11.011>.
- [18] Li LL, Wen SY, Tseng ML, Wang CS. Renewable energy prediction: A novel short-term prediction model of photovoltaic output power. *J Clean Prod* 2019;228:359–75. <https://doi.org/10.1016/j.jclepro.2019.04.331>.
- [19] Das UK, Tey KS, Seyedmahmoudian M, Idna Idris MY, Mekhilef S, Horan B, et al. SVR-based model to forecast PV power generation under different weather conditions. *Energies* 2017;10:1–17. <https://doi.org/10.3390/en10070876>.
- [20] Sheng H, Xiao J, Cheng Y, Ni Q, Wang S. Short-Term Solar Power Forecasting Based on Weighted Gaussian Process Regression. *IEEE Trans Ind Electron* 2018;65:300–8. <https://doi.org/10.1109/TIE.2017.2714127>.
- [21] Liu D, Sun K. Random forest solar power forecast based on classification optimization. *Energy* 2019;187:115940. <https://doi.org/10.1016/j.energy.2019.115940>.
- [22] Wang J, Li P, Ran R, Che Y, Zhou Y. A short-term photovoltaic power prediction model based on the Gradient Boost Decision Tree. *Appl Sci* 2018;8. <https://doi.org/10.3390/app8050689>.
- [23] Mellit A, Sağlam S, Kalogirou SA. Artificial neural network-based model for estimating the produced power of a photovoltaic module. *Renew Energy* 2013;60:71–8. <https://doi.org/10.1016/j.renene.2013.04.011>.
- [24] Zhou Y, Zhou N, Gong L, Jiang M. Prediction of photovoltaic power output based on similar day analysis, genetic algorithm and extreme learning machine. *Energy* 2020;204:117894. <https://doi.org/10.1016/j.energy.2020.117894>.

- [25] Zang H, Cheng L, Ding T, Cheung KW, Liang Z, Wei Z, et al. Hybrid method for short-term photovoltaic power forecasting based on deep convolutional neural network. *IET Gener Transm Distrib* 2018;12:4557–67. <https://doi.org/10.1049/iet-gtd.2018.5847>.
- [26] Lee W, Kim K, Park J, Kim J, Kim Y. Forecasting solar power using long-short term memory and convolutional neural networks. *IEEE Access* 2018;6:73068–80. <https://doi.org/10.1109/ACCESS.2018.2883330>.
- [27] Wang F, Yu Y, Zhang Z, Li J, Zhen Z, Li K. Wavelet decomposition and convolutional LSTM networks based improved deep learning model for solar irradiance forecasting. *Appl Sci* 2018;8:1–30. <https://doi.org/10.3390/app8081286>.
- [28] Sun Y, Szucs G, Brandt AR. Solar PV output prediction from video streams using convolutional neural networks. *Energy Environ Sci* 2018;11:1811–8. <https://doi.org/10.1039/c7ee03420b>.
- [29] Aprillia H, Yang HT, Huang CM. Short-term photovoltaic power forecasting using a convolutional neural network-salp swarm algorithm. *Energies* 2020;13. <https://doi.org/10.3390/en13081879>.
- [30] Han S, Qiao Y, Yan J, Liu Y, Li L, Wang Z. Mid-to-long term wind and photovoltaic power generation prediction based on copula function and long short term memory network. *Appl Energy* 2019;239:181–91. <https://doi.org/10.1016/j.apenergy.2019.01.193>.
- [31] Li P, Zhou K, Lu X, Yang S. A hybrid deep learning model for short-term PV power forecasting. *Appl Energy* 2020;259:114216. <https://doi.org/10.1016/j.apenergy.2019.114216>.
- [32] Ahmed R, Seeram V, Mishra Y, Arif MD. A review and evaluation of the state-of-the-art in PV solar power forecasting: Techniques and optimization. *Renew Sustain Energy Rev* 2020;124:109792. <https://doi.org/10.1016/j.rser.2020.109792>.
- [33] Wang H, Lei Z, Zhang X, Zhou B, Peng J. A review of deep learning for renewable energy forecasting. *Energy Convers Manag* 2019;198:111799. <https://doi.org/10.1016/j.enconman.2019.111799>.
- [34] Wang K, Qi X, Liu H. Photovoltaic power forecasting based LSTM-Convolutional Network. *Energy* 2019;189:116225. <https://doi.org/10.1016/j.energy.2019.116225>.
- [35] Behera MK, Nayak N. A comparative study on short-term PV power forecasting using decomposition based optimized extreme learning machine algorithm. *Eng Sci Technol an Int J* 2019;23:156–67. <https://doi.org/10.1016/j.estch.2019.03.006>.
- [36] Xie T, Zhang G, Liu H, Liu F, Du P. A hybrid forecasting method for solar output power based on variational mode decomposition, deep belief networks and auto-regressive moving average. *Appl Sci* 2018;8. <https://doi.org/10.3390/app8101901>.
- [37] Zhang Y, Zhao Y, Kong C, Chen B. A new prediction method based on VMD-PRBF-ARMA-E model considering wind speed characteristic. *Energy Convers Manag* 2020;203:112254. <https://doi.org/10.1016/j.enconman.2019.112254>.
- [38] Cheng G, Wang Y, Xu S, Wang H, Xiang S, Pan C. Automatic Road Detection and Centerline Extraction via Cascaded End-to-End Convolutional Neural Network. *IEEE Trans Geosci Remote Sens* 2017;55:3322–37. <https://doi.org/10.1109/TGRS.2017.2669341>.
- [39] Wang L, Liu Y, Li T, Xie X, Chang C. Short-term PV power prediction based on optimized VMD and LSTM. *IEEE Access* 2020;8:165849–62. <https://doi.org/10.1109/ACCESS.2020.3022246>.
- [40] Zhang J, Tan Z, Wei Y. An adaptive hybrid model for day-ahead photovoltaic output power prediction. *J Clean Prod* 2020;244:118858. <https://doi.org/10.1016/j.jclepro.2019.118858>.
- [41] Yıldız C, Acıkgoz H, Korkmaz D, Budak U. An improved residual-based convolutional neural network for very short-term wind power forecasting. *Energy Convers Manag* 2021;228:113731. <https://doi.org/10.1016/j.enconman.2020.113731>.
- [42] Korkmaz D, Acıkgoz H, Yıldız C. A Novel Short-Term Photovoltaic Power Forecasting Approach based on Deep Convolutional Neural Network. *Int J Green Energy* 2021;1–15. <https://doi.org/10.1080/15435075.2021.1875474>.
- [43] Demir F, Ismael AM, Sengur A. Classification of Lung Sounds with CNN Model Using Parallel Pooling Structure. *IEEE Access* 2020;8:105376–83. <https://doi.org/10.1109/ACCESS.2020.30000111>.
- [44] DKASC. Alice Springs, 1B: Trina 2020. <http://dkasolarcentre.com.au/source/alice-springs/dka-m9-a-c-phases>.
- [45] Ghimire S, Deo RC, Raj N, Mi J. Deep solar radiation forecasting with convolutional neural network and long short-term memory network algorithms. *Appl Energy* 2019;253:113541. <https://doi.org/10.1016/j.apenergy.2019.113541>.
- [46] Bianco S, Cadene R, Celona L, Napoletano P. Benchmark analysis of representative deep neural network architectures. *IEEE Access* 2018;6:64270–7. <https://doi.org/10.1109/ACCESS.2018.2877890>.
- [47] Landola FN, Han S, Moskewicz MW, Ashraf K, Dally WJ, Keutzer K. SqueezeNet: AlexNet-level accuracy with 50x fewer parameters and <0.5MB model size. *Arxiv* 2016;160207360:1–13.
- [48] Shelhamer E, Long J, Darrell T. Fully Convolutional Networks for Semantic Segmentation. *IEEE Trans Pattern Anal Mach Intell* 2017;39:640–51. <https://doi.org/10.1109/TPAMI.2016.2572683>.